**REVIEW**

# Photochemical Reactions and Photoinduced Electron-Transfer Processes in Liquids, Frozen Solutions, and Proteins as Studied by Multifrequency Time-Resolved EPR Spectroscopy

by **Anton Savitsky** and **Klaus Möbius***

Department of Physics, Free University Berlin, Arnimallee 14, D-14195 Berlin
(phone: +49 30 83852770; fax: +49 30 83856046; e-mail: moebius@physik.fu-berlin.de)

Dedicated to the memory of Professor *Hanns Fischer*

In this overview, modern multifrequency EPR spectroscopy, in particular at high magnetic fields, is shown to provide detailed information about structure, motional dynamics, and spin chemistry of transient radicals and radical pairs occurring in photochemical reactions. Examples discussed comprise photochemical reactions in liquid solution and light-initiated electron transfer processes both in biomimetic donor–acceptor model systems in frozen solution or liquid crystals and in natural photosynthetic-reaction-center protein complexes. The transient paramagnetic states exhibit characteristic electron polarization (CIDEP) effects. They contain valuable information about structure and dynamics of the transient reaction intermediates. Moreover, they are exploited for signal enhancement. Continuous-wave (cw) and pulsed versions of time-resolved high-field EPR spectroscopy, such as cw-transient-EPR (TREPR) and pulsed-electron-spin-echo (ESE) experiments, are compared with respect to their advantages and limitations for the specific system under study. For example, W-band (95-GHz) TREPR spectroscopy in conjunction with a continuous-flow system for light-generated short-lived transient spin-polarized radicals of organic photoinitiators in solution was performed with a time resolution of 10 ns. The increased *Boltzmann* polarization at high fields even allows detection of transient radicals without CIDEP effects. This enables one to determine initial radical polarization contributions as well as radical-addition reaction constants. Another example of the power of combined X-band and W-band TREPR spectroscopy is given for the complex electron-transfer and spin dynamics of covalently linked porphyrin–quinone as well as *Watson–Crick* base-paired porphyrin–dinitrobenzene donor–acceptor biomimetic model systems. Furthermore, W-band ESE experiments on the spin-correlated coupled radical pair $P^{\bullet+}_{865}Q^{\bullet-}_{A}$ in reaction centers of the purple photosynthetic bacterium *Rb. sphaeroides* reveal details of distance and orientation of the pair partners in their charge-separated transient state. The results are compared with those of the ground-state $P_{865}Q_{A}$. The high orientation selectivity of high-field EPR provides single-crystal-like information even from disordered frozen-solution samples. The examples given demonstrate that high-field EPR adds substantially to the capability of 'classical' spectroscopic and diffraction techniques for determining structure–dynamics–function relations of biochemical systems, since transient intermediates can be observed in real time in their *working states* on biologically relevant time scales.

**1. Introduction.** – *Hanns Fischer*, to whoes memory this Special Issue is dedicated, was among the first who performed EPR studies of short-lived transient intermediates of chemical reactions [1][2]. Specifically, he studied radical polymerization in organic solvents by using a fast-flow system. This mixes the reactants just in front of the EPR cavity and, thus, provides fresh sample volumes to be studied. *Hanns Fischer* quickly embarked on the promising combination of EPR and photolysis to study the radicals generated by intense irradiation with UV light while the liquid sample flows through

© 2006 Verlag Helvetica Chimica Acta AG, Zürich

the EPR cavity [3][4]. He and his Ph.D. student *Henning Paul* characterized the transient radical intermediates of photochemical reactions of ketones in solution by their hyperfine couplings and *g* factors, taking advantage of an improved flow system they had constructed allowing for a much smaller consumption of chemicals. *Fischer* and *Paul* were also among the first who observed electron-spin-polarization effects in the EPR spectra of transient radicals in solution, *i.e.*, enhanced absorption and emission of certain hyperfine lines [5][6]. They used their fast-flow system mixing two aqueous solutions, one containing oxidizing $H_2O_2$, the other containing the reducing $Ti^{III}$/EDTA complex (EDTA = *N*,*N*′-ethane-1,2-diylbis[*N*-(carboxymethyl)glycine]) and the organic substance RH (propanoic acid or butanoic acid) [5]. A few examples of phase-inverted hyperfine lines had been previously observed when irradiating organic liquids with energy-rich electrons [6]. And again *Hanns Fischer* was among the first to contribute theoretical models to explain the non-*Boltzmann* behavior of transient radical intermediates [7–10].

*Fischer*'s exciting contributions to the detection and characterization of transient reaction intermediates by EPR spectroscopy employing fast-flow systems and light irradiation had a strong impact on the EPR community in chemistry. Also our multifrequency EPR work at FU Berlin has benefited from *Fischer*'s work over several decades up to now [11–15].

In this contribution, we will present an overview of some of our multifrequency time-resolved EPR studies on photochemical reactions and photoinduced electron-transfer processes in liquid and frozen solutions of organic molecules and proteins. The chosen examples cover the photolysis of some photoinitiators of polymerization reactions in liquid solution, the photoinduced electron-transfer reactions in organic donor–acceptor biomimetic model systems of photosynthesis and, finally, the primary electron transfer in bacterial photosynthetic-reaction-center protein complexes.

**2. CIDEP Mechanisms in Photochemical Reactions.** – The electron-spin system of reactive radicals, as a rule, exhibits chemically induced dynamic electron polarization (CIDEP), *i.e.*, the populations of the spin states deviate from thermal equilibrium. The phenomenon can arise from a variety of mechanisms, and electron-spin polarizations can be created either when the radicals are suddenly initiated or during their bimolecular termination reactions from preferred spin states. A large amount of information on these spin polarizations has been gathered during the past 35 years, and the CIDEP phenomenon has been utilized in numerous studies to get insights into details of radical generation and radical reactions. Many reviews concerning CIDEP effects have been published in recent years. Therefore, in the following only the short overview of polarization mechanisms will be given that are relevant for the photochemical systems described in this work.

2.1. *Triplet Mechanism* (TM). Photochemical radical generation can occur by reaction of singlet excited molecules. Then, the *Zeeman* energy levels $\alpha$ and $\beta$ become equally populated, and the radical system has zero spin polarization immediately after creation. Alternatively, singlet excited molecules may also undergo intersystem crossing (ISC) to their triplet state and form radicals from there. It is well known that the ISC process can lead to differently populated triplet sub-levels [16]. The resulting initial spin polarization of the triplet state can then be transferred to radical-reac-

tion products, provided the decay into radicals occurs fast enough to compete with spin relaxation in the triplet molecule.

The zero-field spin sub-levels of a triplet molecule, $T_x$, $T_y$, and $T_z$ are nondegenerate due to the dipolar or zero-field coupling between the electrons ($x$, $y$, and $z$ denote the principal axes of the zero-field tensor). ISC often occurs, under molecular selection rules, predominantly into one of these states, thus producing triplet molecules with pronounced spin polarization in the molecular frame. This is a commonly observed phenomenon in the solid state, see *e.g.*, [17]. As soon as a triplet is formed, its spin magnetic moment will start to interact with the external magnetic field $B_0$ of the EPR spectrometer. The interaction can transform a substantial part of the molecular-frame spin polarization into a *Zeeman*-level spin polarization with respect to $B_0$ (*i.e.*, in the laboratory frame). The transformation may be envisioned by an adiabatic model in which, after triplet formation, the magnetic field is slowly turned on in such a direction that the highest-energy molecular spin state will evolve into the highest *Zeeman* spin state $T_+$. However, the actual transformation process is more complicated because of essentially two factors. Firstly, the exposure to an external field is not an adiabatic process, as the magnetic field is already present when the triplets are formed, and secondly, in liquids, the orientations of the triplet molecules with respect to the magnetic field are subject to stochastic changes because of rapid rotational diffusion. In fact, the rigorous quantum-mechanical treatment shows [18–22] that the amount of spin polarization which is transferred from the molecular to the laboratory frame depends on the ratio of zero-field splitting (ZFS) and *Zeeman* interaction, $\omega_{ZFS}/\omega_0$, as well as on the rotational correlation time $\tau_R$. Spin polarization vanishes if either $|\omega_{ZFS}/\omega_0| \ll 1$ or $\omega_0 \cdot \tau_R \ll 1$. In both cases, the molecular-frame polarization will be destroyed faster than it is transformed, either by *Zeeman* precession or molecular tumbling. Fortunately, neither of both cases is met for a wide variety of triplet molecules in solutions of low viscosity.

The *Zeeman* polarization will be destroyed by spin–lattice relaxation unless the triplet reacts rapidly to yield a pair of radicals. Spin–lattice relaxation of triplet molecules in solution is very fast because of the strong anisotropic magnetic dipole–dipole interaction between the two triplet spins combined with the rapid change of this interaction as the molecule tumbles in solution. The time scale of this process is of the order of $10^{-8}$ to $10^{-10}$ s [23]. Consequently, the triplet molecule must react on a comparable time scale to transfer a substantial part of the triplet polarization to the radical products. It should be mentioned that even if the *Zeeman* polarization of the triplets has completely relaxed to the equilibrium polarization $p_{eq}$, an excess absorption of $4/3 \cdot p_{eq}$ will be carried to the radicals due to twice the *Zeeman* splitting $g \cdot \mu_B \cdot B_0$ between $T_+$ and $T_-$. This small enhanced absorption, however, is often negligible in comparison with the population differences in the electron-spin levels produced initially in the radical system by the TM effect [24].

2.2. *Radical-Pair Mechanism* (RPM). The radical-pair mechanism (RPM) of CIDEP in liquid solution is more general than the TM in that the radicals do not have to originate from a triplet state. The polarization arises during the radical lifetime as a result of magnetic interactions between radicals when forming spin-correlated radical pairs.

The RPM has three fundamental elements: *1*) The reaction mechanism involves a pair of radicals either created together *via* dissociation or some other reaction of an excited molecule (geminate or G pair), or formed by a random encounter of separately generated radicals (free or F pair). *2*) The reactivity of the radical pair is determined by its electron-spin state which can be singlet, triplet, or some mixture of singlet and triplet states. The radicals in the singlet state will attract each other to form a recombination (or some other) product, whereas the triplet state is repulsive and does not lead to product formation. *3*) The radicals comprising the pair may separate to a point where the short-range valence or exchange forces are negligible. Then magnetic interactions within the radicals (electron-nuclear hyperfine interactions and electron interactions with the external magnetic field) can mix these singlet and triplet states, converting a reactive singlet pair into triplet, and *vice versa*.

The detailed description of the RPM of CIDEP requires application of the stochastic *Liouville* equation (SLE) to describe the evolution of the radical-pair spin state. The resulting models of the process, including a simple vector model which also embodies the effect of spin exchange [25][26], have been described elsewhere [27–29]. However, a simple qualitative picture of the RPM polarization development as well as the polarization rules can be given by using the quasi-adiabatic model of *Adrian* [24][30]. The main assumption of this model is that the separation and re-encounter of the radical pair causes the spin state to evolve partially as it would have if the initial separation of the radicals were very slow (adiabatic). The actually observed polarization is much less than that achievable in the limiting case of adiabatic radical separation. According to theory [31–35], the polarization is approximately given by *Eqn. 1*, where $p(S-T_0)$ is the difference of the probabilities for a radical pair being initially in the $T_0(\alpha_N)$ state to separate as $\alpha\alpha_N,\beta_R$ and $\beta\alpha_N,\alpha_R$, with analogous definitions holding for $T_0(\beta_N)$, $S(\alpha_N)$, and $S(\beta_N)$. Here, $(\alpha,\beta)$ and $(\alpha_N,\beta_N)$ denote the orientation of electron and nuclear spins of the observer radical with respect to the external magnetic field. The hyperfine interaction of the counter radical is considered to be negligible, therefore, only electron-spin projections $(\alpha_R,\beta_R)$ are considered. $D$ is the relative diffusion coefficient of the two radicals forming the pair, and $Q$ is half the difference of their *Larmor* frequencies. The definition of $1/\delta$, the characteristic length of the exchange interaction $J(r)$, follows from its exponential dependence on the radical separation $r$ (*Eqn. 2*), where $d$ is the distance of closest approach. The quantity $d^2/D$ is the time required for the radical pair to diffuse to a distance of closest approach, typically $10^{-12}$ to $10^{-10}$ s. As for realistic systems $\delta\cdot d\gg 1$, *Eqn. 1* yields typical RPM polarizations of $5\cdot 10^{-3}$ to $5\cdot 10^{-2}$ for $\delta\cdot d\approx 4$ and hyperfine splittings of *ca.* 2 mT, *i.e.*, $Q=3.5\cdot 10^8$ rad$\cdot$s$^{-1}$.

$$p(S-T_0)\approx\frac{\pi}{2\cdot\delta\cdot d}\sqrt{\frac{Q\cdot d^2}{D}} \tag{1}$$

$$J(r)=J_0\cdot\exp[-\delta\cdot(r-d)] \tag{2}$$

For the initial, *i.e.*, geminate triplet radical pair, the EPR spectrum of the observer radical appears EA-polarized (low-field EPR lines in emission, high-field lines in enhanced absorption). For the initial singlet pair, the polarization pattern is reversed (AE). F Pairs of radicals form in an initial singlet or triplet state. Usually, these pairs

polarize like triplet-state geminate pairs, because the singlet F pairs are removed by reaction upon the first encounter.

Electron-spin polarization can also be generated at the $ST_-$ level crossing. In this region, the singlet–triplet splitting due to the exchange interaction is balanced by the triplet *Zeeman* splitting. The adiabatic terms avoid the level crossing because of singlet–triplet mixing by the hyperfine interaction, thus causing the initial $T_-(\alpha_N)$ level to be converted to $S(\beta_N)$, and *vice versa*. In contrast to the $ST_0$ mixing, this process produces a net magnetic polarization connected with a change in electron-spin orientation and accompanied by an opposite change in nuclear-spin orientation, as required by the conservation rule of angular momentum.

Starting from an initial triplet state, this process would effectively underpopulate the $\beta\alpha_N$ level and the $\beta_R$ electron-spin level of the counter radical $R^{\bullet}$, because conversion of $T_-(\alpha_N)$ to $S(\beta_N)$ removes $\beta\alpha_N$ as well as $\beta_R$ states and generates additional $\alpha\beta_N$, $\beta\beta_N$, as well as $\alpha_R$ states. In this case, the low-field line is emissively polarized and the high-field line has zero polarization. However, this is the case only for the radical whose hyperfine interaction causes the singlet–triplet mixing. All hyperfine levels of the counter radical ($R^{\bullet}$) are equally polarized. Finally, for an initial singlet radical pair, the polarization pattern will be reversed, *i.e.*, the high-field line will show an enhanced absorption.

The $ST_-$ polarization is generally less important in liquid solutions than $ST_0$ polarization because the $ST_-$ crossing region in high fields is spatially very small compared to the $ST_0$ crossing region, thus limiting the amount of the $ST_-$ mixing. Nonetheless, $ST_-$ polarization can be significant in two cases: *1*) one radical of the pair has a large hyperfine splitting (*e.g.*, P-centered radicals) [36]; *2*) diffusion is slow, and the system spends a relatively long time in the crossing region [37], alternatively the external magnetic field is low enough.

2.3. *Spin-Correlated Radical-Pair Mechanism* (CCRP). Before discussing the TREPR results in some detail, we summarize the theoretical description of correlated coupled radical-pair (CCRP) states [38–41]. After electron transfer, one unpaired spin is localized on the donor site, the other unpaired spin on the acceptor site. The spin dynamics of this radical pair are described by the stochastic *Liouville* equation (SLE) which includes charge separation, recombination, and spin relaxation. The spin Hamiltonian of the system for a specific orientation of the molecule with respect to the external magnetic field $B_0$ is given by *Eqn. 3*, where hyperfine couplings are neglected. The interaction terms are given by *Eqns. 4*,*a–c*.

$$\hat{H} = \hat{H}_{\text{Zeeman}}(\hat{\mathbf{S}}_1) + \hat{H}_{\text{Zeeman}}(\hat{\mathbf{S}}_2) + \hat{H}_{\text{exchange}}(\hat{\mathbf{S}}_1, \hat{\mathbf{S}}_2) + \hat{H}_{\text{dipolar}}(\hat{\mathbf{S}}_1, \hat{\mathbf{S}}_2) \tag{3}$$

$$\hat{H}_{\text{Zeeman}}(\hat{\mathbf{S}}_i) = \mu_B \cdot \hat{\mathbf{S}}_i \cdot \mathbf{g} \cdot \mathbf{B}_0 \tag{4a}$$

$$\hat{H}_{\text{exchange}}(\hat{\mathbf{S}}_1, \hat{\mathbf{S}}_2) = -J \cdot \hbar \cdot (\hat{\mathbf{S}}_2 - 1) \tag{4b}$$

$$\hat{H}_{\text{dipolar}}(\hat{\mathbf{S}}_1, \hat{\mathbf{S}}_2) = \hat{\mathbf{S}} \cdot \mathbf{D} \cdot \hat{\mathbf{S}} = -\frac{2 \cdot D}{3} \cdot \hbar \cdot \hat{S}_z^2 + \left(\frac{D}{3} - E\right) \cdot \hbar \cdot \hat{S}_x^2 + \left(\frac{D}{3} + E\right) \cdot \hbar \cdot \hat{S}_y^2 \tag{4c}$$

Depending on the relative strengths of the various magnetic interactions, some assumptions can be made concerning the proper eigenfunctions. In the high-field limit, when the dipolar and exchange interactions are small compared to the *Zeeman* interaction, the eigenstates of the 4-level system are approximated by the unperturbed triplet states $|T_+\rangle$ and $|T_-\rangle$ and the mixtures $|2\rangle$, $|3\rangle$ of $|S\rangle$ and $|T\rangle$. The amount of state mixing is given in terms of the mixing angle $\varphi_{mix}$ (see *Eqn. 5*).

$$\tan\varphi_{mix} = \frac{\Delta\omega}{J + d/2 + \sqrt{(J + d/2)^2 + \Delta\omega^2}} \tag{5}$$

According to the CCRP model, all four possible one-quantum transitions of light-induced radical pairs have the same intensities because differences in transition moments are compensated by the respective population differences [40][41]. These population differences are due to spin polarization which results from singlet electron transfer as well as from triplet electron transfer, *i.e.*, the populations of the four states differ significantly from *Boltzmann* equilibrium. Thus, for each orientation of the molecule with respect to the magnetic field, two EPR lines in absorption and two lines in emission should be detected, all equal in amplitude. The transient EPR spectra of frozen-solution samples reflect the powder average over all possible orientations. Thus, because of the anisotropy in the magnetic interactions, TREPR spectra contain information about the molecular structure.

For strongly coupled spins, *i.e.*, $|J| \gg |\Delta\omega|$, singlet and triplet are approximately eigenstates, *i.e.*, $|2\rangle \approx |S\rangle$ and $|3\rangle \approx |T_0\rangle$, while for weakly coupled spins, the eigenstates are given by the respective eigenfunctions of each radical. It will be demonstrated that the covalently linked porphyrin–quinone systems of this study form strongly coupled radical pairs.

In particular, strongly coupled systems are sensitive to the deviation of the population differences between the four spin-energy levels that would lead to equal intensities for all the transitions predicted by the CCRP model. Because the transitions to $|S\rangle$ are almost forbidden, only the two allowed transitions contribute to the EPR signal of strongly coupled radical pairs. These two remaining transition frequencies are given by *Eqns. 6*,*a* and *b*.

$$|T_+\rangle \leftrightarrow |T_0\rangle: \quad \omega_{+0} = \frac{1}{2}\cdot\frac{\mu_B}{\hbar}\cdot(g_1(\phi,\theta) + g_2(\phi,\theta))\cdot B_0 + \frac{3}{2}\cdot d \tag{6a}$$

$$|T_0\rangle \leftrightarrow |T_-\rangle: \quad \omega_{0-} = \frac{1}{2}\cdot\frac{\mu_B}{\hbar}\cdot(g_1(\phi,\theta) + g_2(\phi,\theta))\cdot B_0 - \frac{3}{2}\cdot d \tag{6b}$$

Since the inhomogeneous linewidths of the recorded TREPR spectra are larger than the inverse rise time of the spectra, it is justified to assume that the TREPR signal follows instantaneously the spin polarization [42]. Therefore, we simulate the TREPR spectra using kinetic equations for the population of the states and the transition energies given by *Eqs. 6*,*a* and *b*, instead of using SLE.

**3. Time-Resolved EPR Spectroscopy: Experimental Aspects.** – The observation of the EPR spectra of transient paramagnetic species, either radicals or triplets, by using

the laser-flash irradiation depended upon the development of fast EPR spectrometers. Historically, two techniques were established: the first uses continuous-wave (cw)-microwave (mw) irradiation and different sampling methods; the second uses pulsed-microwave irradiation. Both methods have advantages and disadvantages, which may also depend on the specific microwave frequency/magnetic field of the spectrometer. Thus, for any investigated system, one has to choose the optimal method depending on time resolution and sensitivity required. Both EPR techniques were extensively reviewed [43–46], and, therefore, in the following, we only briefly discuss the principles and limitations of them.

3.1. *Continuous-Wave Techniques.* Conventional EPR spectroscopy is performed by means of cw microwaves and up to 100-kHz field modulation with the phase-sensitive detection. The response time of the system is typically tens of microseconds. For certain chemical and biological systems, this time resolution allows already to study radical reactivity. However, it is difficult to detect and follow CIDEP under these conditions mostly because of short electron-spin relaxation times which lead to *Boltzmann* populations of the radical-spin states or, at least, to their partial equilibration, before the radicals can be detected. In the mid 70s, several attempts were made to improve the time resolution of cw EPR to *ca.* 1 μs by using field-modulation frequencies up to 2 MHz [6][47]. Nevertheless, because of still unsufficient time resolution, experimental difficulties to cope with the small penetration depth of the modulation field and the availability of low-noise microwave amplifiers, the cw-EPR method was superseded by the so-called 'direct detection' time-resolved EPR, known as TREPR. In TREPR, the responses of the transient radicals are detected during continuous microwave excitation, but without magnetic-field modulation. The transient EPR signal following the sudden radical generation, *e.g.*, by a laser pulse, is taken at a fixed external-magnetic-field value directly from the microwave bridge mixer or diode detector and collected by using either a transient digitizer or a boxcar signal avarager. The complete EPR spectra are obtained by stepping the external magnetic field through the resonance region.

The time resolution of a TREPR spectrometer is limited by the response time which determines how fast the spectrometer can follow changes of the EPR absorption of the sample that occurred in the microwave cavity. In general, any change of the perpendicular magnetization $v(t)$ will result in a change of the spectrometer output signal $S(t)$ which is given by the convolution integral of $v(t)$ with the response function $f(t)$ of the instrument: $S(t)=f(t)\otimes v(t)$. The response function of the detection instrument is given by the response characteristics of the microwave and amplification circuitry. In the absence of any additional restriction of the microwave detection and amplification circuitry, the response time of the EPR instrument is generally determined by the bandwidth of the EPR cavity. The reflection coefficient of a critically coupled cavity (here we discuss only the common reflection mode spectrometer) is given by *Eqn. 7*, where $Q_L$ is the loaded-quality factor of the cavity and $\nu_0$ is the spectrometer frequency [48]. Thus, the EPR absorption signal appearing at frequency $(\nu-\nu_0)$ will be filtered by the cavity as given by $\sqrt{(1-|\Gamma|^2)}$ in the frequency domain. After *Fourier* transformation of the filtering function, one obtains the response function of the cavity in the time domain, *Eqn. 8*, where $T_R$ is the ringing time of the EPR cavity. Actually, this ringing time gives the physical limit of the EPR-instrument response time. It should be men-

tioned that the rise time of EPR signals is not given only by the response time defined above but by a physical limitation for cw-TREPR detection: The concentration of transient radicals typically reaches its maximum at the end of the laser flash, when the ensemble magnetization is not yet tipped away from the $z$-axis by the cw-microwave field.

$$|\Gamma|^2 = \frac{\varepsilon^2}{4+\varepsilon^2} \quad \text{with} \quad \varepsilon = 4 \cdot Q_L \cdot \frac{\nu - \nu_0}{\nu_0} \tag{7}$$

$$f = \exp[-t/T_R] \quad \text{with} \quad T_R = Q_L \cdot (\pi \cdot \nu_0)^{-1} \tag{8}$$

As follows from *Eqn. 8*, the ringing time $T_R$ of the EPR cavity is inversely proportional to the microwave frequency of the EPR spectrometer. Fixing a typical loaded quality value $Q_L = 2000$ of a single-mode EPR cavity, $T_R = 240$, 67, and 6.7 ns can be calculated for S-band ($\nu_0 = 2.7$ GHz), X-band ($\nu_0 = 9.5$ GHz), and W-band ($\nu_0 = 95$ GHz) EPR, respectively. Thus, the typical time resolution of X-band TREPR spectrometers is *ca.* 50–100 ns, which is much longer than the laser-pulse duration of typically 5 ns. At W-band, however, the response time is below 10 ns and becomes adequate for the pulsed laser experiments. The time resolution of X-band TREPR could be improved by using cavities with a low quality factor. However, normally this is not the method of choice. Decreasing the cavity quality factor leads directly to a decrease of the EPR signal [49] and, thus, to lower sensitivity of the EPR experiment.

The sensitivity of a TREPR experiment is proportional to the ratio of the signal amplitude to the noise amplitude in the direct detected mode. The signal amplitude depends on the radical system under study, *i.e.*, on the amount of mw absorption due to the magnetization of transient paramagnetic species created during or after their generation. The magnetization can be increased by optimization of the experimental conditions, for example, laser-light intensity, sample size. The noise amplitude of TREPR is determined by three contributions: *i*) the noise of the microwave detection and amplification circuitry; *ii*) the noise of the microwave source; *iii*) reproducibility of the experimental conditions for each laser shot, *i.e.*, laser-light intensitiy, temperature, sample bleaching, *etc*. The first contribution determines the 'noise floor' of the EPR spectrometer. The noise floor is independent of the incident microwave irradiation. It is generally measured by the noise figure and the amplification gain of the detection network. The noise figure describes the loss of the useful signal intensity on the way from the EPR cavity to the end detector, for example, due to losses in waveguides and mixer elements, accompanied by the gain of noise intensity in the amplifier elements. The typical noise figure of modern EPR spectrometers is around 5. It can hardly be improved without resorting to microwave elements operating at cryogenic temperatures. The second contribution is more crucial for the success of the TREPR experiment. The quality of the microwave source is characterized in terms of amplitude and phase noise. The phase noise describes the width of the microwave radiation in the frequency domain, *i.e.*, the mw power at frequency offsets ($\nu - \nu_0$) from the carrier frequency ($\nu_0$). The amplitude noise is the fluctuation of this mw power. The noise power, if reflected from the EPR cavity, reaches the detector and increases the noise amplitude. For cw EPR, this noise is less important because the cavity serves as a filter at typical frequency offsets up to 100 kHz (see *Eqn. 7*), corresponding to the frequency

of the field modulation. TREPR, however, uses broadband detection to be able to follow fast signal changes. The cavity reflects 50% of the incident microwave power at the frequency offset $(\nu - \nu_0)$ corresponding to $\nu_0/Q_L$ (see *Eqn. 7*). If the microwave noise is high enough, starting from a certain excitation power, its collective contribution to the spectrometer-noise amplitude will overide the noise floor, then linearly increasing with increasing of microwave amplitude. Thus, in this situation, no signal-to-noise-ratio improvement can be obtained by increasing the mw power because the EPR signal depends on the amplitude of the excitation microwave as well. Improved microwave technology in the past years resulted in commercial low-noise microwave sources and power amplifiers. Nevertheless, care should be taken to choose the proper bandwidth of the detection circuitry to minimize the contribution of microwave-source-noise to the overall-noise amplitude.

The study of formation and decay kinetics of transient radical species requires not only the best possible time resolution but also the ability to adequately analyze the EPR signals. While TREPR provides an excellent time resolution, especially when going to high mw frequencies, it has a number of negative characteristics concerning data analysis. First, the time development of the EPR spectra is governed by the continous interaction between the spin system and the cw-microwave field. The perturbation shows up by the strong time dependence of the EPR linewidth in the time domain when the inverse of the time delay between radical formation and signal detection becomes comparable to the intristic linewidth of the EPR signal. This can prevent spectra detection or radical identification at early times after radical formation. Second, the microwave radiation field also influences the time evolution of the EPR signals. In addition to the usual kinetic parameters of the chemical reaction and spin relaxtion as well as of radical dynamics and CIDEP production, the time development of the EPR responses is strongly influenced by the mw field strength in the cavity. It does not only dominate the signal rise but can also produce an oscillatory behavior of the signal. As the result, the determination of rate parameters from TREPR spectra is commonly based on modified *Bloch* equations that, in addition to spin and chemical dynamics, also account for the perturbation of the system by the microwave field. Generally, the analysis involves a nonlinear, multiparameter least-squares fit of the experimental data to the numerical solution of a set of differential equations [50][51]. The equations are based on an *a priory* model accounting for all the processes that play a role in the spin evolution. Only in rare cases, it is possible to simplify the data analysis (see below). Additionally, the influence of the mw field strength often has the consequence that TREPR measurements can cover only the time period during which the spin system is far from thermal equilibrium. However, the last problem can be overruled by going to high microwave frequencies (see below).

The problem of continuous perturbation of the spin system by the cw-microwave irradiation that complicates the analysis of TREPR data can be avoided by applying pulsed EPR techniques. We note, however, that cw-microwave irradiation of the sample has also a positive aspect: It allows to perform TREPR and cw-EPR experiments simultaneously. A small (compared with the EPR linewidth) magnetic-field modulation does not perturb fast TREPR responses, but can be used for parallel phase-sensitive signal detection to observe long-lived radical-reaction products which are not detectible by TREPR.

3.2. *Pulsed EPR Techniques.* Pulsed EPR methods such a *Fourier*-transform (FT) EPR and electron-spin-echo (ESE) spectroscopy have become well established in the last years [43][52][53]. In these techniques, the magnetization along the external-field direction ($z$ magnetization) associated with formation and decay of transient radicals is monitored by turning the magnetization vector in the transverse ($xy$) plane with one or more short microwave pulses, followed by the detection of EPR responses in the absence of the excitation microwave field.

There are two advantages of pulsed methods compared to TREPR. First of all, the detection happens without incident microwave power. Thus, the noise signal in pulsed experiments is determined by the noise floor of the spectrometer and by the stability of experimental conditions, *i.e.*, becomes independent of mw-source noise. Second, the measured EPR response is directly proportional to the $z$ magnetization existing at the moment of mw excitation. This simplifies data analysis because the excitation microwave field has not to be included in the analysis model.

Besides advantages, there are two serious limitations which are connected to each other, time resolution and sensitivity. The time resolution of pulsed techniques is determined by the time from the start of the detection mw-pulse sequence to the moment at which the EPR response can be recorded. It consists on two contributions: *i*) the length of the pulse sequence and *ii*) the dead time of the EPR spectrometer.

In FT-EPR, the pulse sequence consists only of one $\pi/2$ mw pulse followed by measuring the free induction decay (FID). The pulse length required for a $\pi/2$ pulse, assuming the *Larmor* frequency of the spin to be equal to the chosen mw frequency, is given by *Eqn. 9*, where $\gamma$ denotes the gyromagnetic ratio of the electron spin. The field amplitude $B_1$ is a function of the available mw excitation power and the power-to-field-conversion efficiency of the EPR resonator. In a real experiment, however, the pulse length is also strongly influenced by the bandwidth of the EPR cavity. The $B_1$ field is not created immediately after switching on the microwave power, but grows in with the ringing time constant $T_R$ of the cavity, see *Eqs. 7* and *8*. Thus, for an X-band spectrometer equipped with a cavity with a loaded-quality factor $Q_L$ of 2000, it is impossible to create pulses shorter than *ca.* 60 ns, even when enough mw power is available. At low mw frequencies, this problem can be overcome by lowering the quality factor of the cavity. This, unfortunately, results in fairly low power-to-field-conversion efficiency as well as in reduced sensitivity. At higher mw frequencies, this limitation becomes less critical. Thus, at W-band and $Q_L = 2000$, pulses as short as 6 ns can be generated. Moreover, the conversion efficiency is much higher at high mw frequencies, because the $B_1$ field is concentrated in a smaller volume of the cavity. Thus, to create a $\pi/2$ pulse of 10 ns length at X-band, *ca.* 1 kW microwave power is required ($Q_L \approx 100$), whereas at W-band, *ca.* 500 mW is already sufficient ($Q_L \approx 2000$).

$$\tau_{\pi/2} = \frac{\pi}{2} \cdot \frac{1}{\gamma \cdot B_1} \tag{9}$$

The EPR response cannot be measured immediately after switching off the microwave power because of the cavity ringing. Thus, one has to wait for a certain time until the ringing microwave has decayed approximately to the level of the expected EPR response. This time is called the dead time of the spectrometer. For X-band, this

time typically amounts to *ca.* 100 ns. At higher frequencies, for instance W-band, the dead time is typically one order of magnitude shorter, profiting from the lower mw excitation power required and from the faster cavity ringing.

The dead time of an EPR spectrometer not only limits the time resolution of pulsed experiments but also limits its applicability to certain radical systems. The FID decay is governed by the linewidth of the EPR signal. The rate of exponential damping of the FID signal ($1/T$) is related to the full width at half height of an EPR line, $\Delta B_{1/2}$, *e.g.*, for a Lorentzian line $\Delta B_{1/2} = 2/\gamma \cdot T$. Thus, for the FID decay to be slower than the spectrometer dead time, the X-band FID technique cannot be used for studies of paramagnetic-system resonance widths larger than 0.1 mT. In contrast to FID, the decay of an ESE response is only determined by the homogeneous linewidth of an EPR transition, *i.e.*, by the $T_2$ relaxation time. On the other hand, an inhomogeneous broadening of the EPR transition is required for the echo formation.

Pulsed EPR probes the full magnetization of the sample and not only transient contributions as TREPR does. If some persistent or long-lived (on the time scale of the experiment) paramagnetic species are generated or initially present in the sample, their EPR responses are also detected by pulsed EPR. In this case, to obtain solely the EPR spectra of the transient radicals, one has to perform additional measurements to get rid of background signals.

Thus, the applicability of the pulsed EPR techniques depends strongly on the investigated radical system. Under proper conditions, pulsed techniques can provide better sensitivity as compared to TREPR. Additionally, the time after radical generation, at which the spin system can be probed, is not limited in pulsed EPR. The probing mw pulses can be placed at any time delays after radical generation yielding undistorted EPR spectra. This is in contrast to the detection of the TREPR spectra of transient radicals: At delay times which exceed the characteristic time window of excitation microwave field, *i.e.*, $1/\omega_1$, TREPR becomes unfeasible. The probing microwave pulses, however, can be placed at any time delays after radical generation yielding undistorted EPR spectra.

The comparison of the transient EPR techniques can be summarized as follows:

*1.* The TREPR method is applicable to all kinds of radical systems both in liquid and frozen solutions. However, the analysis of the experimental data is complicated due to continuous perturbation of the spin system by the microwave field. For the same reason, the detection of undistorted transient EPR signals on delay time scales $> 1/\omega_1$ is often impossible.

*2.* The applicability of FT-EPR spectroscopy is restricted to transient radical systems having an overall EPR linewidth less than the dead time of the spectrometer. This condition is typically fulfilled only for radical systems in liquid solution of low viscosity.

*3.* The spin-echo techniques require inhomogeneously broadened EPR lines. Therefore, the strength of ESE-EPR is particularly pronounced for the investigation of radicals in frozen solutions (generally in solids). The $T_2$ relaxation time and/or chemical decay kinetics of the detected species should be slower than the dead time of the EPR spectrometer.

The main advantages of the transient EPR experiments at high magnetic fields/microwave frequencies are: *i*) high time resolution; *ii*) high spectral (*Zeeman*) resolu-

tion; *iii*) possibility to detect transient radicals even in their thermally equilibrated state.

**4. Applications.** – 4.1. *Photochemical Reactions in Liquid Solution*. Since the early 70s, EPR methods were extensively applied to characterize the transient radicals in liquid-solution reactions. Time-resolved EPR techniques have been applied to a wide variety of photochemical systems, including investigations of radical reaction kinetics, identification and characterization of reaction intermediates, elucidation of reaction mechanisms with regard to the spin states involved. One broad area of EPR studies was to investigate the chemical reactivity of radicals, especially concerning the radical–radical recombination, as well as addition reactions of the radicals to other chemical compounds. The addition reactions are of crucial importance for the coating industry as well as for medicine. The second field of applications is to study spin-polarization (CIDEP) effects and spin-relaxation dynamics in radical systems. In the following, we demonstrate, by means of two photochemical systems, the power of multifrequency EPR in reaction and spin chemistry of radicals in liquid solution. Some of the presented results were obtained by combined efforts of Austrian, German, and Swiss EPR groups and were published recently [11][12][54]. Other results are presented here for the first time.

The 2,2-dimethoxy-1,2-diphenylethan-1-one (DMPA) is an industrial agent for efficient photocuring (*Iragacure® 651*, *Ciba Speciality Chemicals*, *Inc.*, Switzerland) used mainly for acrylic and unsaturated polyester/styrene resins. Due to its technical relevance, the DMPA photochemistry has been subject of many investigations [55–58], including EPR experiments [12][59][60]. The photochemical behavior of DMPA was, for a long time, in the focus of interests of *Hanns Fischer*. The first EPR investigation of DMPA photocleavage was performed in his laboratory at the University of Zürich employing the cw X-band EPR technique [61], followed by time-resolved X-band EPR experiments [59]. Finally, in 1990, he published a comprehensive analysis of radical reactions induced by DMPA photodissociation, applying product analysis, chemically induced dynamic nuclear polarization (CIDNP), and optical and EPR techniques [58], thereby clarifying also discrepancies of previous measurements.

The primary steps of photolysis of DMPA consist of singlet excitation and fast intersystem crossing (ISC) to its triplet state, immediately ($\tau_T < 100$ ps) followed by *Norrish*-type-I photocleavage of the triplet, yielding benzoyl and dimethoxybenzyl radicals, $R^1$ and $R^2$, respectively (see *Fig. 1,a*). The quantum efficiency of the triplet cleavage is higher than $\Phi > 0.7$ (dependent on solvent) [56]. The radicals $R^1$ and $R^2$ appear highly electron-spin polarized. This polarization originates from the triplet (TM) and radical-pair (RP) mechanisms (see *Sect. 2*). Because of this, the DMPA photolysis was used at FU Berlin as test system for the CIDEP-enhanced ENDOR experiment [13] to test Q-band time-resolved EPR [60] and, recently, to develop sophisticated methods for the analysis of EPR spectra with overlap of several signals at X-band [62].

We found the DMPA system to be very suitable for the first test of our W-band TREPR spectrometer equipped with a continuous-flow system for light-generated short-lived organic radicals in solution [12]. The W-band EPR spectra obtained after photolysis of 65 mM DMPA in $O_2$-free benzene solution are shown in *Fig. 1,b* for several time delays after the laser flash. For comparison, the X- and Q-band spectra pre-

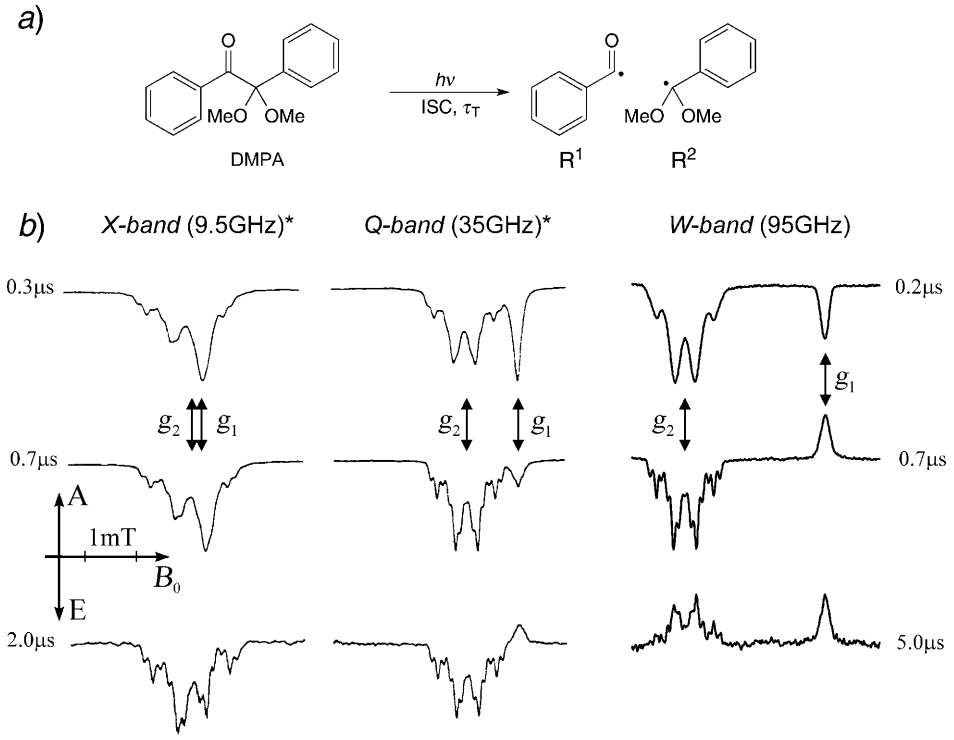


Fig. 1. a) *Reaction scheme for the primary steps of the photolysis of DMPA in liquid solution.* b) *X-, Q-, and W-band time-resolved EPR spectra taken at delay times indicated after flash photolysis* (352 nm) *of 65 mM* (W-band) *DMPA in benzene at room temperature.* The X- and Q-band spectra (marked by *) are adapted from [60].

viously reported by *Forbes* [60] are also shown. At W-band, the high-field TREPR spectra of the benzoyl and dimethoxybenzyl radicals $R^1$ and $R^2$, respectively, appear completely resolved owing to the significant difference of their $g$ values, $g_1 = 2.00690 \pm 0.00005$ and $g_2 = 2.00295 \pm 0.00005$, respectively. Directly after the laser flash, the spectra of both radicals appear in net emission at all microwave frequencies and *Zeeman* fields. This indicates that TM CIDEP dominates. However, the amount of initial emissive polarization of $R^1$, compared to that of $R^2$, decreases with increasing field. This is not unexpected: On the one hand, the polarization due to $\Delta g$-RPM CIDEP in the initial radical pair increases with increasing field, giving rise to enhanced absorption of radical $R^1$ and emission of $R^2$. On the other hand, the net emissive polarization, which the radicals gain from the triplet precursor, gets smaller at higher fields (see below), thereby enhancing the contribution of $\Delta g$-RPM. The increasing $\Delta g$-RPM polarization in F pairs of $R^1$ and $R^2$ has been proposed to be responsible for the phase inversion (emission to absorption) of the benzoyl-radical signals at later times in Q-band EPR [60]. This argument should also hold for W-band EPR. However, this is not the only possible explanation: The W-band EPR spectra, recorded 5 μs after laser irradiation, show that both signals appear in absorption. This strongly suggests

that in this situation, the radicals are observed in their thermal (*Boltzmann*) equilibrium. The equilibrium polarization $P_{eq}=\frac{1}{2}\cdot g\cdot\beta_e\cdot p_{eq}\cdot N_A\cdot x_i/x$ ($N_A=$*Avogadro*'s number, $x_i/x=$weight factor of the EPR transition under study) is proportional to the population difference $(N_\alpha-N_\beta)$ between the two *Zeeman* levels $\alpha$ ($S_Z=+1/2$) and $\beta$ ($S_Z=-1/2$) in *Boltzmann* equilibrium (see *Eqn. 10*), taking into account that $h\cdot\nu_0\ll kT$. At room temperature, $p_{eq}$ corresponds to *ca.* $7.8\cdot10^{-4}$ for $\nu_0=9.5$ GHz (X-band), and to $7.8\cdot10^{-3}$ for $\nu_0=95$ GHz (W-band). Thus, in X-band EPR, the same initial population difference decays to a 10 times smaller magnitude than in W-band EPR. This means that, if the radical system starts with a net polarization corresponding to a population difference of the two *Zeeman* levels of, say, $(N_\alpha-N_\beta)/(N_\alpha+N_\beta)=0.1$ both at X- and W-band, after relaxation and in the absence of chemical reactions, the observed signal contains only *ca.* 0.8% of initial polarization in X-band, but 8% in W-band. Thus, the observed phase inversion is caused both by $\Delta g$-RPM in F pairs and by increased equilibrium polarization at high magnetic fields.

$$p_{eq}=\frac{N_\alpha^0-N_\beta^0}{N_\alpha^0+N_\beta^0}\approx\frac{h\cdot\nu_0}{2\cdot kT} \tag{10}$$

The results of this first multi-frequency investigation of DMPA photolysis allows us to realize the following: *i*) For a full understanding of the polarization mechanisms in the radical system, it is necessary to study the system at different microwave frequencies; *ii*) at high magnetic fields, it is possible to observe the radicals in their thermally equlibrated state, *i.e.*, *Bolzmann*-polarized. This chance to observe, by TREPR at high fields, transient radicals in thermal equilibrium opens new perspectives for investigations of CIDEP phenomena and radical kinetics. First of all, there is now the possibility for direct determination of initial polarization, since the initial signal can be scaled to the thermally equilibrated one. Secondly, analysis of the time dependence of the EPR time profiles may yield directly the kinetic information about the radical reactions.

To demonstrate the power of multi-frequency EPR in spin chemistry studies as well as in investigations of radical reactions, we next examined the photolysis of another polymerization photoinitiator of the acylphosphine oxide type: diphenyl(2,4,6-trimethylbenzoyl)phosphine oxide (TMDPO). It is a highly efficient curing agent which is industrially (*Darocur® TPO*, *Ciba Speciality Chemicals*, *Inc.*, Switzerland) used to initiate radical photopolymerization in unsaturated resins such as those based on a prepolymer in combination with single- or multifunctional monomers. The photochemistry of TMDPO is well established [63–65]. According to the scheme in *Fig. 2*, photolysis of TMDPO yields 2,4,6-trimethylbenzoyl ($R^3$) and diphenylphosphinoyl ($R^4$) radicals *via Norrish*-type-I cleavage ($\Phi\approx0.6$) from short lived ($\tau_T<1$ ns) triplet excited state, formed from the photoexcited singlet *via* ISC.

W-, X-, and S-Band transient EPR spectra after laser-flash photolysis of TMDPO in benzene solution are shown in *Fig. 3*. The spectra consist of three lines: the inner line stems from the C-centered radical $R^3$, and the outer two lines are due to the P-centered radical $R^4$ (see *Fig. 2*). From the W-band spectrum, the P-hyperfine coupling, which splits the EPR spectrum of radical $R^4$ in two lines, was determined as $(36.25\pm0.05)$ mT. The $g$ values, $g_3=2.00055\pm0.00005$ and $g_4=2.00412\pm0.00004$, were obtained by

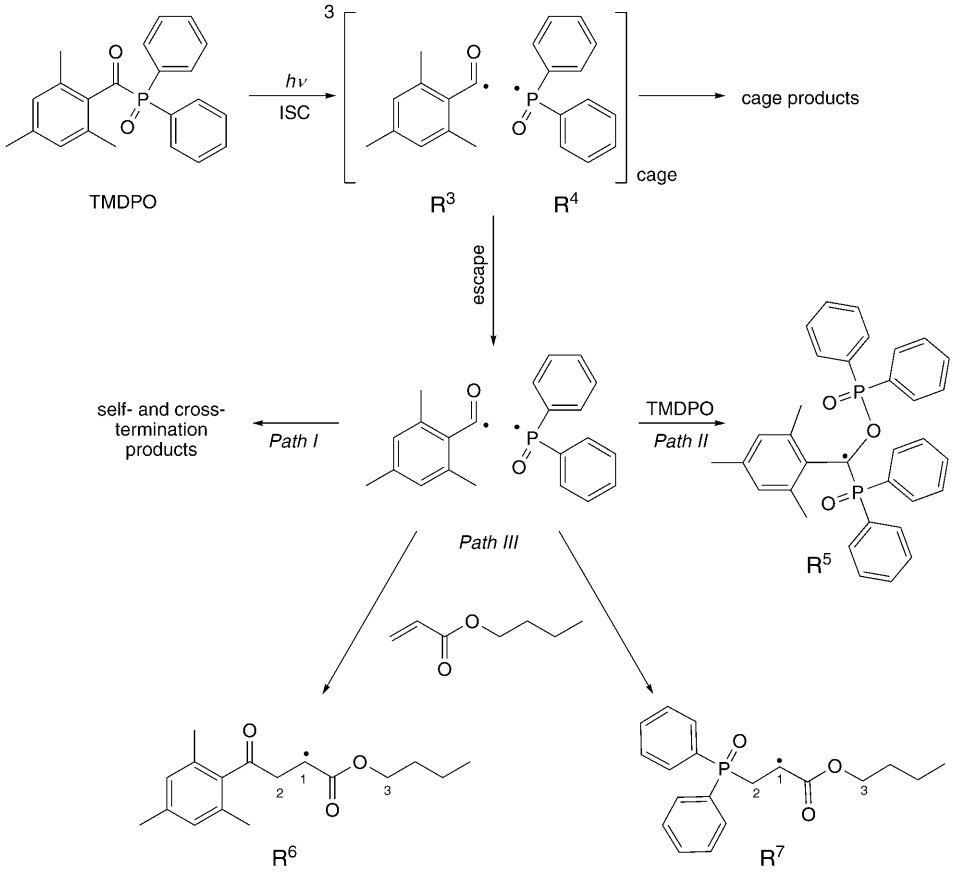


Fig. 2. *Reaction scheme for the primary and secondary steps of the photolysis of TMDPO.*

W-band EPR for radicals $R^3$ and $R^4$, respectively. The deviation of these values from the earlier reported ones, 2.0008 and 2.0035, in benzene at X-band [65] has, probably, to be attributed to insufficient accuracy of these X-band data. The difference in *g* values corresponds to a magnetic resonance field offset of *ca.* 6 mT at W-band, but only of *ca.* 0.6 mT at X-band, which is close to the linewidth (see *Fig. 3*). Another source of errors are second-order effects on the resonance positions, which become pronounced at low EPR frequency bands. For example, in S-band the splitting between low- and high-field lines of the diphenylphosphinoyl radical $R^4$ was *ca.* 37.5 mT, which is 1.25 mT larger than its hyperfine splitting (see *Fig. 3*). At high fields the second-order effects are suppressed. Hence, high-field EPR enables a more accurate determination of *g* factors and hyperfine-splitting constants of different transient radicals in solution.

At short delay times after the laser flash, the W-band TREPR spectra of $R^3$ and $R^4$ exhibit net absorptive polarization (see *Fig. 3*). For the diphenylphosphinoyl radical $R^4$, in addition a multiplet polarization of the EA type (low-field line in emission/high-field line in absorption) is revealed, as is apparent from the different intensities of the low-

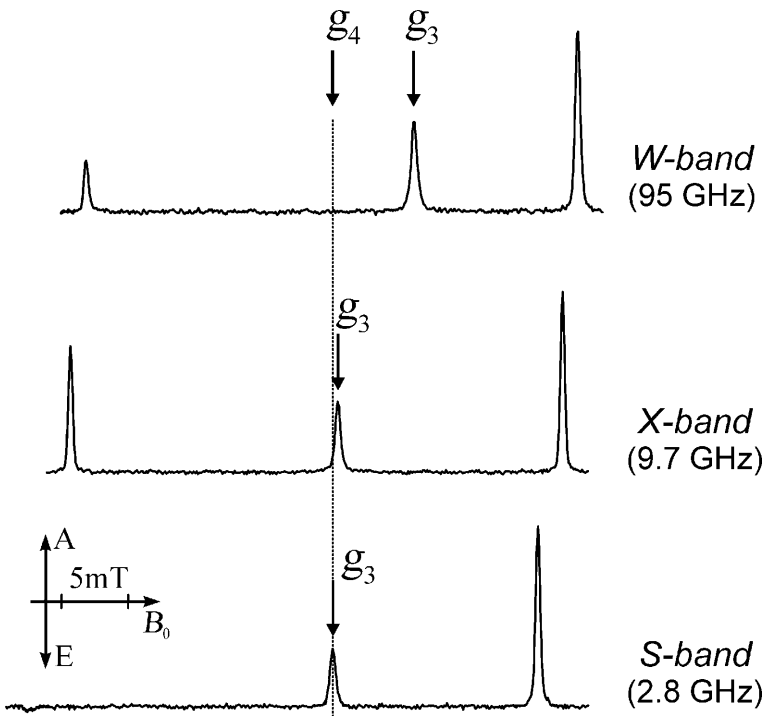


Fig. 3. *Time-resolved EPR spectra of $R^3$ and $R^4$ recorded at different microwave frequencies after laser-flash photolysis* (355 nm) *of TMDPO in benzene at room temperature with a time delay of 200 ns.* For details, see [11].

and high-field lines. The net absorption observed for both radicals reflects the TM polarization transferred from excited TMDPO. The second contribution to the net polarization of radicals comes from the $\Delta g$-RPM in the geminate triplet radical pairs (RPs) of $R^3$ and $R^4$. For the benzoyl radical $R^3$, the $\Delta g$-RPM contribution is positive (absorption), and, for the diphenylphosphinoyl radical $R^4$, it is negative (emission) since $g_3 < g_4$. The EA multiplet polarization contribution in the spectrum of $R^4$ is generated by $ST_0$-mixing of the radical-pair mechanism ($ST_0$-RPM) in the geminate RPs of $R^3$ and $R^4$. The initial polarization pattern of the radicals is different in all EPR bands (S-, X-, W-band), which is clearly seen in *Fig. 3*. This difference is explained in terms of a field dependence of the CIDEP-generating mechanisms. For example, the initial multiplet $ST_0$-RPM polarization is, to a good approximation, magnetic-field-independent [33][34][66]. However, the polarization due to $\Delta g$-RPM and TM changes when going from W- to S-band EPR. At long times after the laser flash, the difference between spectra taken at different microwave frequencies becomes more dramatic. At X-band, the enhanced absorption observed for $R^4$ decays within *ca.* 1 μs after the laser flash, leaving the spectrum purely multiplet-polarized (low-field line in emission/high-field line in absorption). However, at W-band, the intensities of both high- and low-field lines become equal after the same delay. Both lines appear in absorption which slowly decays to zero. To explain this phenomenon, the EPR time profiles of the

high- and low-field lines of $R^4$, as observed in X- and W-band, were compared [12]. The time profiles were analyzed in terms of net and multiplet contributions, which were obtained by adding and subtracting the intensities of the low- and high-field resonances of $R^4$, respectively. At X-band, the observed picture is well described by the CIDEP mechanisms and the reaction scheme mentioned above. The initial net absorption from TM and $\Delta g$-RPM decays with the spin–lattice relaxation time $T_1$, as does the multiplet polarization contribution that was initially gained in the geminate pairs of radicals $R^3$ and $R^4$ by $ST_0$-RPM. At later times, due to the spin-selective recombination of radicals $R^4$, according to *Path I* in *Fig. 2*, the $ST_0$-RPM in F pairs of radicals $R^4$ give rise to the multiplet polarization. There is no production of net polarization at later times by $\Delta g$-RPM, because no recombination of $R^3$ and $R^4$ takes place, due to the different reactivity of both radicals [63]. Thus, as expected, in X-band, the net EPR signal intensity decays faster than the multiplet EPR intensity. The slow decay of the net polarization at W-band cannot be explained by field-dependent changes of the relaxation times $T_1$ and $T_2$ of radicals $R^4$ because such changes should be reflected equally by the net and multiplet signals. Thus, it can only be explained by the equilibrium polarization, because the initial net polarization does not decay to zero, but to the thermally equilibrated one, see above.

The time profile of net-polarization contribution at W-band can be analyzed by using the analytical solution of the *Bloch* equations that account for initial net polarization and first-order chemical reaction [12] (see *Eqn. 11*), if the conditions $T_2 \ll T_1$, $\omega_1^2 \ll T_1^{-1} \cdot T_2^{-1}$, and $T_1/\tau \ll 1$ are fulfilled. Here, $\omega_1$ is the microwave-field amplitude, $P_{eq}$ the radical equilibrium polarization, $[R]_0$ the initial radical concentration, and $\tau$ the first-order lifetime constant with intact TMDPO (see *Path II*, *Fig. 2*); $P_n$ is the net polarization contribution in units of $P_{eq}$. The conditions for *Eqn. 11* were found to be fulfilled for $R^4$. The best agreement with experiment was found for $P_n = 8.5 \pm 1$, $T_1 = 600 \pm 50$ ns, and $1/\tau = k_1 = (1.7 \pm 0.3) \cdot 10^5\ s^{-1}$. The individual fits were obtained with reduced $\chi^2$ factors between 1.1 and 1.4, demonstrating the quality of the data.

$$v(t) = P_{eq} \cdot [R]_0 \cdot \omega_1 \cdot T_2 \cdot \left[e^{-t/\tau} + (P_n - 1) \cdot e^{-t/T_1}\right] \tag{11}$$

The possibility to read out the chemical lifetime of $R^4$ from W-band EPR time profiles allows to study the addition reaction of diphenylphosphinoyl radicals to functional monomers. This possibility, which additionally served for testing our approximations, was used to investigate the addition reaction of $R^4$ to butyl acrylate (= butyl prop-2-enoate; BA), *Path III* in *Fig. 2*. *Fig. 4* depicts the cw and TREPR spectra taken in the absence and in the presence of 0.5M BA with the stem toluene solution of 48 mM TMDPO. In the absence of BA (*Fig. 4,a*) the TREPR spectra demonstrate the behavior described above. In the cw-EPR spectra, the signals of long-lived radicals are observed. One of the signals around $g = 2.00288$ is assigned to a C-centered radical $R^5$ formed by the reaction of $R^4$ with intact TMDPO, according to *Path II* in *Fig. 2*, establishing that $R^4$ disappears *via* pseudo-first-order kinetics. The hyperfine couplings of $R^5$, $A(P1) = 2.87$ mT, $A(P2) = 1.79$ *m*T, and $A(H) = 0.13$ mT, were in good agreement with previously reported values (2.82, 1.67, and 0.13 mT, resp.) [65]. An addition rate constant of $R^4$ to TMDPO of $3.5 \cdot 10^6\ s^{-1} \cdot M^{-1}$ is estimated from $k_1$ and the TMDPO concentration. Radical $R^5$ is not observed in the sample containing BA (*fig. 4,b*). The unre-

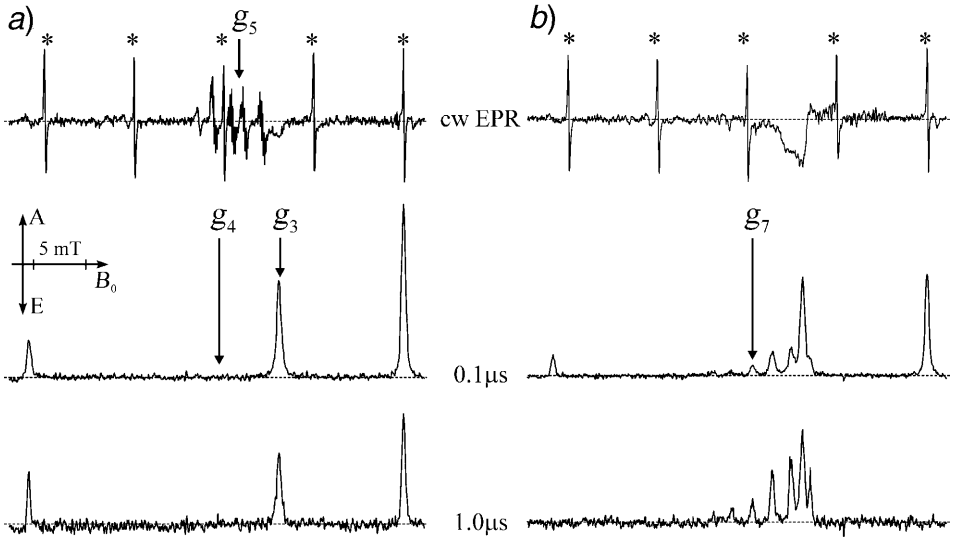


Fig. 4. *W-Band cw and time-resolved EPR spectra observed after photolysis of* a) *48 mM TMDPO and* b) *48 mM TMDPO and 0.5M butyl acrylate in toluene solution at 298 K*. The cw and TREPR spectra were taken simultaneously with a magnetic-field modulation amplitude of 5 μT. The asterisks mark the signals of the $Mn^{2+}$ field standard which is positioned in the microwave cavity.

solved signal around $g=2.005$ observed in the cw-EPR spectrum is probably due to a mixture of radicals from the polymerization chain reaction. At 0.1 μs after the laser flash, the TREPR spectrum shows the signals of $R^3$ and $R^4$; however, the ratio of the EPR intensities changes in favor of the benzoyl radical $R^3$. Additionally, the signal of the adduct radical $R^7$ appears. At longer times, 1 μs in *Fig. 4,b*, the $R^4$ signal disappears but is accompanied by a growing of the $R^7$ signal. The signal due to $R^3$ decays approximately with the same rate constant as in the BA-free sample. The hyperfine parameters of radical $R^7$ centered at $g_7=2.0033$, $A(P)=5.8$ mT, $A(H(1),H(2))=1.93$ mT, and $A(H(3))=0.2$ mT, were determined from simulation of the TRPER spectra.

The net signals of $R^4$ at low BA concentrations demonstrate a biexponential decay character according to *Eqn. 11*. At BA concentrations above 100 mM, the signals decay monoexponentially (see *Fig. 5,a*). The simultaneous fit of the net decay profiles to *Eqn. 11*, varying only the chemical-lifetime constant, provided the $\tau$ values in *Fig. 5,b*. Analysis of the data dependence in terms of *Eqn. 12* yields a second-order-addition rate constant for $R^4$ addition to BA of $k_{add}=3.2\cdot10^7\ s^{-1}\cdot M^{-1}$ for low adduct concentrations. The rate constant $k_{add}$ is in a good agreement with the values $2.8\cdot10^7\ s^{-1}\cdot M^{-1}$ [67] in MeCN and $3.3\cdot10^7\ s^{-1}\cdot M^{-1}$ [64] for addition to methly methacrylate in hexane that were obtained by laser flash photolysis (LFP). However, it is slightly higher than the values $1.8\cdot10^7\ s^{-1}\cdot M^{-1}$ and $2\cdot10^7\ s^{-1}\cdot M^{-1}$ determined in toluene from the analysis of X-band TREPR linewidth broadening and LFP experiments [68]. At high BA concentrations (>250 mM), the measured reciprocal chemical-lifetime values significantly deviate from a linear dependence from [BA], see *Fig. 5,b*. The recent investigation of the addition reaction of differently substituted benzoyl radicals to BA established two domains

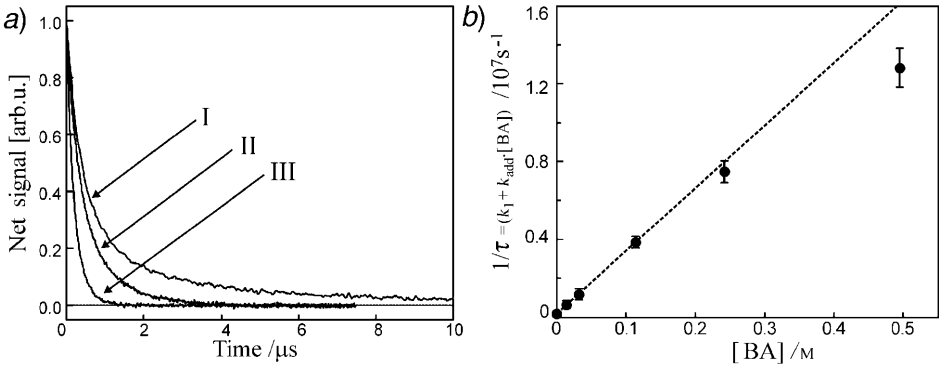


Fig. 5. a) *Net polarization/time profile of radical* $R^4$ *observed in the absence of BA* (I) *and in the presence of 32 mM* (II) *and 114 mM* (III) *BA in the sample toluene solution.* b) *Plot of the inverse chemical lifetime* $1/\tau$ *of* $R^4$ vs. *BA concentration, as determined from the fits of net polarization/time profiles.* The dashed line gives a linear fit for BA concentrations below 250 mM.

of radical reactivity in dependence on concentration of BA [54]. At alkane concentrations above 1M, the addition reaction is slowed down by about one order of magnitude. This decrease coincides with a dramatic increase of the macroscopic viscosity of the reaction medium. We suggest that the same increase of viscosity is responsible for the slowing down of the addition reaction of $R^4$ to BA. This also can explain the difference between values obtained by *Gescheidt*, *Rist*, and co-workers [68], which were measured for BA concentrations between 0.5 and 2M.

$$1/\tau = k_1 + k_{add} \cdot [BA] \tag{12}$$

Thus, the analytical solution of the *Bloch* equation (*Eqn. 11*), was found to be valid for the examined system. The example given above demonstrates the power of high-field EPR for obtaining detailed information on radical reactions in solution. The possibility to observe the radicals in their thermally relaxed state allows to follow their chemical kinetics directly. Moreover, high time resolution of high-field EPR allows to measure the short radical chemical lifetimes from EPR signal decays. For example, the EPR signal of $R^4$ in solution containing 0.5M BA decays with the time constant of *ca.* 70 ns (*Fig. 5*, *b*). This value is already comparable with the time resolution of conventional X-band EPR spectrometers. It is, however, about a factor of 10 lower than the time resolution of our W-band spectrometer, see *Sect. 2*.

The analysis of the net EPR signals yields, besides the chemical lifetime of the radicals, also the initial net polarization $P_n$ in absolute units. For the determination of the initial multiplet polarization, $P_m$, the ratio of the net and multiplet EPR intensities, at short times after the laser pulse, was used. It was assumed that on the given time scale, either spin relaxation or chemical reaction influences net and multiplet polarizations differently. A ratio $P_n/P_m = 1.55 \pm 0.15$ was found. Thus, the initial W-band net and multiplet CIDEP magnitude of the diphenylphosphinoyl radical system after photolysis of TMDPO is obtained. The radicals are produced with the net polarization $P_n = 8.5 \pm 1$, which corresponds to an initial population difference $P_n \cdot p_{eq}$(W-band) = 0.066. This net

polarization is superimposed by multiplet polarization (EA) of $P_m = 5.5 \pm 0.8$, which is equivalent to 0.043 in terms of population difference. Because only triplet and radical pair mechanisms are responsible for the production of the initial multiplet and net polarizations in $R^4$, the values obtained at W-band can be used to determine the absolute polarizations at lower frequencies. The experiments at S- (2.7 GHz), X- (9.5 GHz) and Q-bands (35 GHz) give the field dependence of the ratio $P_n/P_m$ of $R^4$ under the same experimental conditions [11]. Analysis of these ratios in terms of the TM and the RP mechanism by $ST_0$, $ST_-$, which becomes extremely important at low fields, yielded the absolute values of triplet polarization which $R^4$ gains from the polarized TMDPO triplet (*Fig. 6*). The observed values of TM polarization are extremely high. They exceed the equilibrium polarization 410 times at 9.5 GHz and nearly 1000 times at S-band.

The magnetic-field strength or microwave frequency is an important parameter that determines the efficiency of spin-polarization transfer from the molecular frame of the excited triplet molecule to the laboratory frame and then to the radicals. Qualitatively, the effect of microwave frequency on the magnitude of the TM polarization is well understood. However, now it becomes possible also to check the theory quantitatively. The field dependence of TM polarization was examined by comparison with the numerical solution of the stochastic *Liouville* equation (SLE) which describes the evolution of the spin system (for details see [11]). In the first step, the parameters of the TMDPO triplet state (triplet lifetime, zero-field splittings, and initial triplet population) obtained previously from X-band EPR investigations were used. A triplet rotational correlation time of 48 ps was estimated from the spherical approximation of the molecule by the *Debye–Stokes* formula. *Fig. 6* presents the experimental dependence of the TM on microwave frequency and the dependence calculated from the SLE (filled circles) by using the triplet parameters from the literature [69]. It is obvious that the TM polarization is underestimated. The field dependence, however, is reproduced correctly. Next, the SLE numerical solution was fitted to the experimental data with the reorientational correlation time and initial population of the $T_z$ state as variable parameters, see *Fig. 6* (open circles). The optimum fit requires a slightly higher population of the $T_z$ level (1.0 instead of 0.8) as well as an increase of the correlation time by a factor of 2 (98 ps, instead of 48 ps). It is reasonable that the correlation time is not equal to the one estimated from the simplified spherical approximation. The rotational diffusion of the molecule is a complex anisotropic process. Therefore, the rotational correlation time should be considered only as an effective parameter.

The numerical solution of SLE explains the observed experimental TM polarization quite well. To check the validity of approximate analytical formulas derived by *Atkins–Evans* [21] and *Pedersen–Freed* [22], TM polarization was calculated with the triplet parameters obtained above (see *Fig. 6*, dashed and dotted lines, resp.). It was found that both approximations are valid only at high microwave frequencies (beyond X-band), although the *Atkins–Evans* approach remains qualitatively correct also at low mw frequencies and magnetic fields. Investigations of the TM polarization of two other acryloylphosphine oxide photoinitiator systems confirm the experimental results of the TMDPO system and their theoretical analysis [11]. Moreover, the parameters of the excited triplet state of phenylbis(2,4,6-trimethylbenzoyl)phospine oxide could be extracted from the dependence of its TM polarization on microwave frequency.

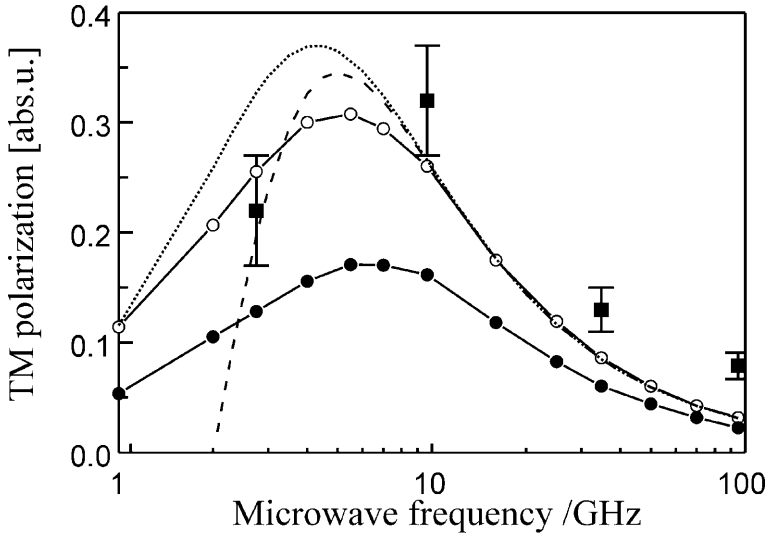


Fig. 6. *TM Polarization of phosphinoyl radical* $R^4$ (■) *after photolysis of TMDPO in comparison with the theoretical calculations* (●) *invoking the numerical solution of the stochastic* Liouville *equation* (SLE) *and by using the triplet-state parameters from* [69] *and triplet rotational correlation time from a spherical approximation;* (○) *best fit of the numerical solution of SLE for the lifetime of the triplet state and its initial population given in the text.* The dashed and dotted lines show the polarization calculated by analytical expressions of *Atkins–Evans* [21] and *Pedersen–Freed* [22] with the parameters of (○). The figure is adopted from [11].

4.2. *Photoinduced Electron Transfer in Biomimetic Model Systems.* 4.2.1. *Preamble.* Understanding the structure–dynamics–function relationship of light-induced electron transfer (ET) in the natural photosynthetic apparatus at atomic level is a fascinating, but extremely difficult task. To resolve this task is not only challenging in its own right but also in view of possible implications for the design of artificial solar energy conversion systems with high quantum efficiency. Long-lived charge-separated radical pairs (RPs) occur as secondary ET intermediades of the light-driven cascade of transmembrane ET steps in the photosynthetic reaction center (RC) protein complex. Because of the complexity of the natural RC – which during evolution was optimized by following strategies not only for high-yield photoinduced charge separation but also for efficient protection against internal and external stress factors – supramolecular organic donor (D)–acceptor (A) model complexes have been synthetized in many laboratories to mimic essential features of photosynthetic ET and, hopefully, to simplify the task of understanding its mechanism (for more recent reviews, see [70–73]). It is established by now that multicomponent biomimetic model complexes (D–s–A), consisting of donor and acceptor moities linked by a spacer (s), can be designed – and synthetized – to produce, with high quantum yield, long-lived charge-separated RPs in homogeneous media like isotropic or liquid crystalline solvents [70][71]. Such supramolecular biomimetics consist of a chromophore that absorbs in the VIS spectral region, and several tailor-made substituents linked to it by covalent bonds or H-bond networks, thus establishing a spacer bridge to provide electronic coupling between

the donor and acceptor moieties. The synthesis of such supramolecular D–s–A complexes generally adheres to strategic principles: The redox potentials of the substituents are chosen in a way to be operative either as electron acceptors or donors. In other words: The substituents will either accept electrons from the photoexcited chromophore or donate electrons to the chromophore after it became oxidized by ejecting an electron from its excited state. By varying the number of substituents as well as the bonding characteristics and spatial arrangement of the spacer, the factors governing long-range ET can be selectively controlled to ultimately stabilize the charge-separated donor–acceptor RP state against energy-wasting charge-recombination reactions. As chromophore, an extended $\pi$-electron system is normally chosen, *e.g.*, a porphyrin moiety, but also for acceptors extended $\pi$-electron systems, such as free-base porphyrins or fullerenes, are favorably chosen for stabilizing the charge-separated state against recombination. This stabilization can be further increased by adding secondary acceptors to the D–s–A dyads, thereby creating supramolecular triads, tetrads, *etc.* [71][72][74]. The characteristics of the linkage between D and A, *e.g.*, $\sigma$-bonds, H-bonds, ligation, or electrostatic interaction, will affect the electronic coupling, $V^2$, between donors and acceptors, ranging from covalent through-bond, *via* direct through-space to superexchange coupling situations. This is similar to what occurs in natural photosynthetic systems along the various ET pathways in the protein.

Thus, the electronic and spatial properties of the spacer decide about the magnitude of the electronic coupling matrix element, $V$, between donor cation and acceptor anion within the charge-separated RP state. Controlling charge recombination (CR) *via* $V_{CR}$ is essential for retarding wasteful ET recombination dynamics also in biomimetic devices, in analogy to what is operative in natural photosynthesis. Unfortunately, determining reliable values of $V_{CR}$ is difficult, both experimentally and theoretically. There exist only a few spectroscopic methods by which $V_{CR}^2$ can be measured indirectly through the exchange coupling parameter $J$ between the electron spins of the radicals within a radical pair. Among these methods are nanosecond transient absorption measurements of magnetic-field effects on the reaction yield [75][76] and nanosecond time-resolved EPR detection of transient spin-polarized radical-pair spectra (TREPR, see above and [77–81]).

The TREPR method excels by providing reliable estimates of the exchange interaction $J$ from the spectral-simulation routines of the spin-polarized spectra of charge-separated spin-correlated RPs in their triplet state. The theoretical analysis of the relation between the singlet–triplet splitting within the RP, $2J = E_S - E_T$, and the electronic coupling, $V_{CR}^2$, goes back to *Anderson* [82] and was later adapted to charge-recombination ET reactions of the RP [75][76][79][80]. According to theory, $2J$ is given by *Eqn. 13*, where $V_n^2$ are the squared electronic coupling matrix elements between the ground state and nearby excited states, weighted by the energy separation $\Delta E_n$ between the RP state and those excited states $n$ to which it is coupled at the nuclear coordinate of the relaxed equilibrium nuclear configuration of the charge-separated RP. The energy gap is given by $\Delta E_n = \Delta E + \lambda$, *i.e.*, by the free energy difference $\Delta E$ for the reaction and the total reorganization energy $\lambda$ for the electron transfer. The individual terms in the equation for $2J$ may have positive or negative signs, depending on the sign of the energy denominator, thereby determining the coupling to be ferromagnetic ($J < 0$) or antiferromagnetic ($J > 0$). Thus, from combining TREPR and cyclic vol-

tammetry experiments, the desired quantity $V^2_{CR}$ can be determined after estimating the solvent reorganization energy $\lambda(r)$ from the size of the donor and acceptor molecules and the dielectric properties of the solvent [83] according to *Eqn. 14*, where $r$ is the center-to-center separation of the D and A molecules, and $d_A$ and $d_D$ are the radii of the D and A molecules (assumed to be spherical). The vacuum permittivity constant, the refractive index, and dielectric constant of the solvent are represented by $\varepsilon_0$, $n_S$, and $\varepsilon$, respectively. We see that from TREPR experiments, crucial information about the D–s–A coupling schemes, for instance direct *vs.* superexchange coupling, can be revealed.

$$2J = E_S - E_T = \left[\sum_n V_n^2/\Delta E_n\right]_S - \left[\sum_n V_n^2/\Delta E_n\right]_T \tag{13}$$

$$\lambda(r) = \frac{e^2}{4\pi\cdot\varepsilon_0}\cdot\left(\frac{d_A}{2}+\frac{d_B}{2}-\frac{1}{r}\right)\cdot\left(\frac{1}{n_S^2}-\frac{1}{\varepsilon}\right) \tag{14}$$

An important aspect of biomimetic long-range ET is the strategic selection of the solvent matrix in which the redox partners are embedded. Intramolecular ET can occur when the photoexcited reactant D, which is linked to A by a spacer s, *D–s–A, moves on a free-energy surface until it reaches a cross-over point with another intersecting surface which corresponds to the final state, *i.e.*, to the charge-separated product $D^{+\bullet}$–s–$A^{-\bullet}$. Once curve crossing occurs, the charge distribution in the molecular complex changes, and the solvation equilibrium will be perturbed. Dielectric relaxation will realign the solvent molecular electric dipoles until – with a characteristic time constant, the *Debye* relaxation time $\tau_D$ of the solvent – a new equilibrium with respect to the new charge distribution is obtained [84]. According to *Marcus*' electron-transfer theory [83] (see below) the controlling factors of the ET rate $k_{ET}$ are both the energetics of the redox couple, *i.e.*, the *Franck–Condon* factor $F$, and the electronic coupling matrix element $V^2$ between donor and acceptor. $F$ is governed by the free energy change $\Delta E$ of the reactants and the reorganization energy $\lambda$ of the final charge-separated state in the equilibrium solvent configuration of the initial state: $F=\exp[-E_a/kT]/\sqrt{4\pi\cdot\lambda\cdot kT}$ with the activation energy $E_a=(\Delta E+\lambda)^2/4\cdot\lambda$.

For fast solvent relaxation dynamics, where the nuclear motion is fast on the ET time scale (nonadiabatic ET), the ET rate is given by $k_{ET}(na)=(2\pi/\hbar)\cdot V^2\cdot F$ [85], where (na) stands for nonadiabatic. The critical quantity describing whether the solvent relaxation (approximated by one relaxation time $\tau_L$) is fast on the ET time scale, is the adiabaticity factor $\kappa$ in *Marcus*' theory: $\kappa=4\pi\cdot V^2\cdot\tau_L/\hbar\cdot\lambda$. In ET processes, two limiting cases are generally considered, the nonadiabatic case with $\kappa\ll 1$, and the adiabatic case with $\kappa>1$. In the adiabatic case (a), the solvent dynamics cannot be neglected, and the ET rate becomes solvent-controlled, *i.e.*, $k_{ET}$ (a) is governed by the solvent's longitudinal dielectric relaxation time $\tau_L$. Consequently, the basic nonadiabatic ET rate, as is prevailing for photosynthetic ET in protein RCs at room temperature, has to be corrected for describing the adiabatic case: $k_{ET}(a)=k_{ET}(na)/(1+\kappa)$. The temperature dependence of $\tau_L$ is determined by the temperature dependence of the *Debye* relaxation time $\tau_D$, since $\tau_L=(\varepsilon_\infty/\varepsilon_s)\cdot\tau_D$. Here, $\varepsilon_s$ and $\varepsilon_\infty$ are the static and high-frequency (optical) dielectric constants of the solvent medium, respectively.

An experimental handle to control the transition from the nonadiabatic to the solvent-controlled adiabatic limit is provided by the temperature and by the choice of the solvent matrix [70]. To monitor the transients of light-induced ET processes by time-resolved EPR, such a matrix control is a prerequisite. It must slow down the normally sub-nanosecond-fast photoinduced ET near room temperature in biomimetic DA systems dissolved in isotropic solution into the time window of transient EPR, which is restricted to, say, 10 ns upwards (see above). Generally, in isotropic solvents, the attenuation of ET processes from a fast nonadiabatic regime into the slower adiabatic regime can be achieved by lowering the temperature to the soft-glass region [86], where the ET process has not yet been frozen out, or by using highly viscous solvents. It is intriguing, however, that anisotropic liquid-crystal (LC) solvents are often the better choice allowing to study the ET transient intermediates over the wide temperature range of the nematic mesophase of the LC, where molecular motion still prevails resulting in well-resolved EPR spectra [87]. The inherent properties of LCs dial the relevant ET rates into the readily monitored $10^6\ s^{-1}$ range.

The clue of explaining this ability of LCs to retard dramatically ET rates is the change of the internal electric field, which accompanies the intramolecular ET. It produces a nematic potential which hinders molecular reorientation [88], thereby prolonging $\tau_D$ in the nematic mesophase of the LC, $\tau_D$(nem), as compared to the *Debye* relaxation time $\tau_D$(iso) in isotropic media: $\tau_D(\text{nem}) = G \cdot \tau_D(\text{iso})$ with the retardation factor $G$ [89], *i.e.*, $G = (\exp[q/kT] - 1) \cdot q/kT$, where $q$ is the barrier height of the nematic potential. The power of LCs as solvents for studying the transient ET reaction intermediates in artificial photosynthetic DA complexes by time-resolved EPR has been widely recognized [39][70][71][77][90–92]. These studies show how by employing LCs with different polarity, viscosity, structure, and diamagnetic susceptibility anisotropy, the ET and spin dynamics can be affected, allowing for a better understanding of the controlling factors of intra- and intermolecular ET reactions in artificial photosynthesis model complexes.

It is clear by now that such studies of model systems provide complementary information also to *in vivo* studies – and *vice versa*. In most of our multifrequency time-resolved EPR studies, we had concentrated on biomimetic DA complexes that are covalently linked by selected spacer groups. These complexes were synthetized by *H. Kurreck* (FU Berlin) and his group in collaboration with whom also our TREPR studies were performed. These studies mainly deal with dyad and triad porphyrin–spacer–quinone systems to elucidate their ET and spin dynamics during light-induced charge-separation and -recombination processes involving transient triplet and radical-pair states. We include also DA models which are not covalently linked, but rather linked by H-bonding networks, thus mimicking more realistically the natural RC situation. These compounds were synthetized in the group of *J. L. Sessler* (Austin, Texas). They involve preorganized supramolecular porphyrin–quinone or porphyrin–nitrobenzene aggregates that are functionalized by appropriate guanine and cytosin residues to allow for molecular recognition *via Watson–Crick* base pairing. The multifrequency TREPR studies were done in collaboration with *H. Levanon* (Hebrew University Jerusalem) and his group. In the following, we will review a few of these experiments taking prominent examples from both types of supramolecular biomimetics.

4.2.2 *Covalently Linked Porphyrin–Quinone Dyad and Triad Model Systems.* 4.2.2.1. *Experimental Results.* Employing 9.5-GHz and 95-GHz TREPR spectroscopy, four different porphyrin (P)–quinone (Q) systems covalently linked by a *trans*-cyclohexyane-1,4-diyl (*trans*CH) bridge (see *Fig. 7*) have been investigated to study the effect of molecular dynamics on electron-spin polarization and light-driven electron-transfer characteristics [39]. The reaction scheme for P-*trans*CH-BQ (BQ = 1,4-benzoquinone = cyclohexa-2,5-diene-1,4-dione) for light-initiated ET [93] is depicted in *Fig. 8*. By absorbing a photon $h\nu$, the (tetraphenylporphyrinato)zinc ([Zn(tpp)]) is excited to its first excited singlet state $P^{S1}$. At room temperature, fast singlet-ET produces the singlet radical-pair (RP) state, $(P^{+\bullet}\text{–}Q^{-\bullet})^{S}$. Since the singlet charge-recombination (SRC) rate $k_{SRC}$ is larger than $10^8\,s^{-1}$ for most porphyrin–quinones, the singlet-RP has decayed before singlet–triplet mixing can generate any detectable EPR-signal intensity. At lower temperatures, however, singlet-ET is slowed down and, hence, spin-orbit intersystem crossing in the porphyrin moiety to the excited triplet state $P^{T*}$ can compete. Subsequently, triplet-ET to the triplet-RP state, $(P^{\bullet+}Q^{\bullet-})^{T}$, can occur. This RP state is detectable by TREPR in polar solvents in a temperature window of *ca.* 30° below the melting point of the solvent. Alternatively, the triplet-RP can be observed over a wider temperature range in the soft-glass phase of the room-temperature liquid crystal *E7* (*Merck*, UK) [89]. At considerably lower temperatures, ET is frozen out, and the EPR spectrum of $P^{T*}$ is observed. In the reviewed work [39], it was shown that the investigated $(P^{+\bullet}\text{–}Q^{-\bullet})^{T}$ triplet-RPs are all strongly coupled, *i.e.*, the exchange interaction $|J| \gg |\Delta\omega|$ with $\Delta\omega = (\mu_B/2\hbar) \cdot B_0 \cdot [g_1(\phi,\theta) - g_2(\phi,\theta)]$. Here $\phi$ and $\theta$ denote the polar angles of the magnetic $\mathbf{B_0}$ field with respect to the molecule in the principal axes system of the zero-field tensor. Moreover, in the chosen solvent matrix, the overall tumbling motion of the complexes is slowed down such that the anisotropic contributions to the zero-field and *g* tensors are resolved in the EPR spectra. Nevertheless, small-angle fluctuations inside the solvent cage prevail and lead to spin–lattice relaxation that is anisotropic, *i.e.*, the reaction rates and chosen transfer pathways depend on the orientation of the molecule with respect to the external magnetic field. These fluctuations also lead to a pronounced modulation of the isotropic exchange interaction *J* affecting the singlet–triplet ($ST_i$, $i = 0, -1, +1$) mixing efficiency. Hence, the TREPR spectra are sensitive not only to molecular structure but also to molecular motion, thereby probing the flexibility and micro-environment of the molecule.

When comparing the present PQ systems with the bacterial photosynthetic reaction center, several points should be mentioned: First, the radical pairs of the PQ systems resemble the secondary RP in RCs rather well because in both cases, the individual radicals are nondiffusing on the EPR time scale, and their anisotropic interactions are resolved by TREPR. Second, in the RC, charge recombination is slow, the RP is only weakly coupled, and the TREPR spectrum can be described by using the correlated-coupled-radical-pair (CCRP, see above) model [94][95]. For example, by analyzing 95-GHz TREPR signals on the basis of the CCRP model, relative orientations of donor and acceptor sites in the RC could be revealed with high accuracy [96]. For strongly coupled RPs, TREPR was observed to be sensitive to motion and relaxation of freely diffusing biradical chains [97–99]. In this case, the exchange interaction is modulated when the chain is folding. In contrast to these cases, here we describe the

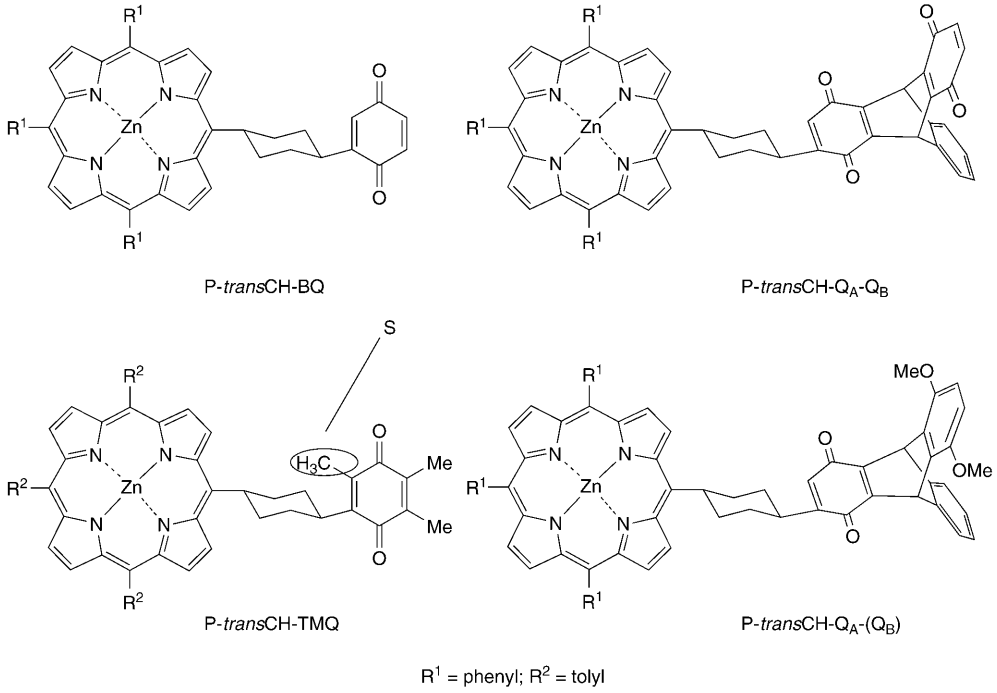


Fig. 7. *Molecular structure of investigated porphyrin–quinone dyad and triad model systems.* P = porphyrin, Q = quinone, BQ = 1,4-benzoquinone, TMQ = 2,3,5-trimethyl-1,4-benzoquinone. *trans*-CH = *trans*-cyclohexane-1,4-diyl. The Me substitution that restricts the motion about the bond between *trans*CH and Q is indicated by S ('bulky' PQ).

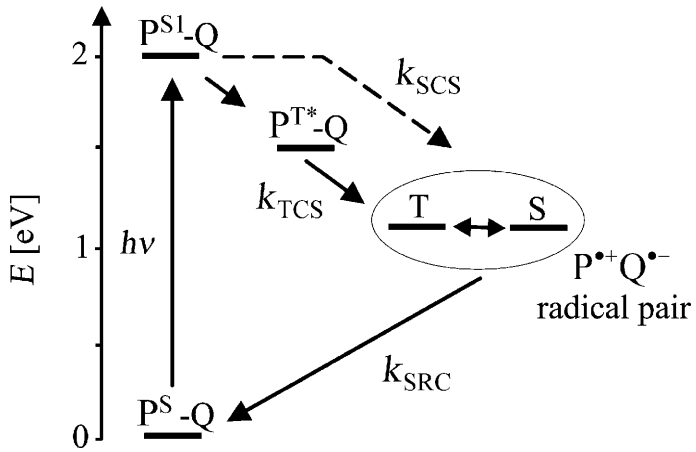


Fig. 8. *Scheme for light-induced electron transfer in the porphyrin–quinone dyad P-*trans*CH-BQ.* The rate $k_{SCS}$ denotes the singlet charge-separation, $k_{TCS}$ the triplet charge-separation, and $k_{SRC}$ the singlet charge-recombination rate. For abbreviations, see *Fig. 7* and text.

dramatic effects of spin relaxation and modulation of $J$ on TREPR line shapes in highly viscous solvents where anisotropic contributions of the spectral parameters are resolved. The results indicate possible misinterpretations of spin and ET dynamics that may occur when performing TREPR experiments at one microwave frequency only.

In *Fig. 9* the X- and W-band spectra of two different PQ systems are shown. They are measured in EtOH and in an EtOH/toluene mixture, *ca.* 10° below the melting point, 1 μs and 5 μs after the laser flash. For delay times longer than 1 μs, the lineshapes remain unchanged and the signal decays within 10 μs. *Fig. 10,a* shows the time evolution of the X-band spectrum of P-*trans*CH-TMQ. It turns out that the PQ systems can be divided into two categories that are related to molecular flexibility. Systems in which the quinone carries no Me substituent next to the cyclohexane-1,4-diyl spacer have totally emissive TREPR spectra. We term them 'nonbulky' PQs. Systems with such an additional Me group (indicated by S in *Fig. 7*) exhibit TREPR spectra which have emissive (E) and absorptive (A) parts. We refer to them as 'bulky' PQs. On cooling the nonbulky systems down to 140 K in EtOH, the spectra become equal to the EEAA spectra of the bulky systems. This was observed before [100], both at X-band and at W-band, and a polarization mechanism for the nonbulky PQs was suggested on the basis of a dynamic exchange interaction due to the higher flexibility of the nonbulky quinone [101]. For the bulky PQs, it was suggested that the X-band spectra may be understood in terms of the CCRP model of weakly coupled radical pairs. A simulation based on that model with $J = -1.15$ mT and $D = -2.3$ mT is shown as dotted line in *Fig. 9,c*. However, for W-band EPR, the CCRP model predicts, on the low-field side, resolved spectral contributions from the quinone anion radical due to its relatively large $g$ value. However, these contributions are not observed at W-band, and the predicted lineshape is totally different from the experimental result (*Fig. 9,d*). Additionally, it was shown by X-band saturation recovery experiments that the polarization is generated within the radical pair, and is not due to polarization transfer from the triplet $P^{T*}$ precursor or due to the CCRP mechanism [102]. It was suggested that the bulky PQs form strongly coupled radical pairs, and the polarization is caused by relaxation phenomena. This suggestion is now supported by the $T_1$ measurements on the dimethylbenzoquinone anion radical at W-band. In the following, we discuss a reaction model on the basis of a strongly coupled RP which includes relaxation. It leads to the convincing simulations of the spectra shown in *Fig. 10,b*. All the TREPR results, both at X- and W-band, on bulky PQs can be understood in terms of this model [39].

4.2.2.2. *Reaction Model for Bulky PQs.* Several mechanisms exist which can produce spin polarization in a strongly coupled radical pair, and population/depopulation pathways involved are depicted in *Fig. 11*. We shall discuss them in the following.

*Triplet Mechanism*: The $P^{T*}$ (porphyrinatozinc) precursor triplet states $|T^p_-\rangle$, $|T^p_0\rangle$ and $|T^p_+\rangle$ are selectively populated by inter-system crossing according to the contribution of $|T^p_Z\rangle$ to these states. This spin polarization is transferred to the RP if the ET rate is large compared to the spin–lattice relaxation rate $W_1$ of the precursor, which is between $6 \cdot 10^6$ and $2 \cdot 10^7$ $s^{-1}$. The EEAA TREPR spectra cannot be due to the triplet mechanism for the following reasons: *i*) their rise time is larger than the decay time of the precursor triplet signal, *ii*) the saturation recovery measurements show that polarization is produced within the RP [102], and *iii*) the triplet mechanism produces spin

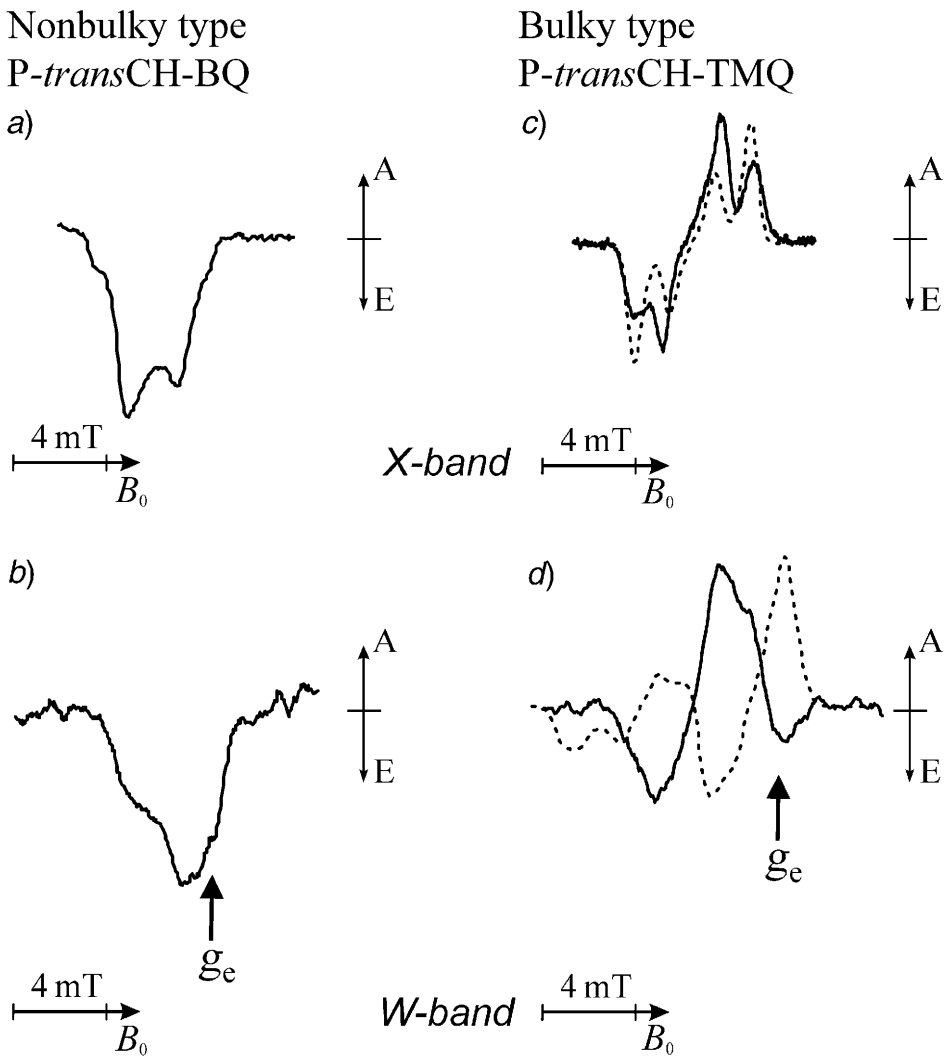


Fig. 9. *TREPR Spectra* (solid lines) *of P-*trans*CH-BQ and P-*trans*CH-TMQ* a) *in EtOH at 150 K* b)–d) *and in EtOH/toluene at 166 K. a*) X-band, 5 μs after laser excitation [131]; *b*) W-band, 5 μs after laser excitation; *c*) X-band, 1 μs after laser excitation [100]; *d*) W-band, 5 μs after laser excitation. The integration time was 1 μs. The letters A and E stand for absorption and emission, respectively. The resonant position for the *g* value of the free electron, $g_e$, is indicated in the W-band spectra. The spectra simulations in *c*) and *d*) (broken lines) are calculated for a weakly coupled radical pair by using the CCRP model, for triplet electron transfer, for $J = -1.1$ mT and for $D = -2.3$ mT and are based on the X-ray structure [108].

polarization symmetric to the porphyrin *Z* axis, which is the PQ dyad's *Y* axis. The spectra simulations show that, instead, the AE spectra that are observed shortly after the laser pulse are due to triplet mechanism.

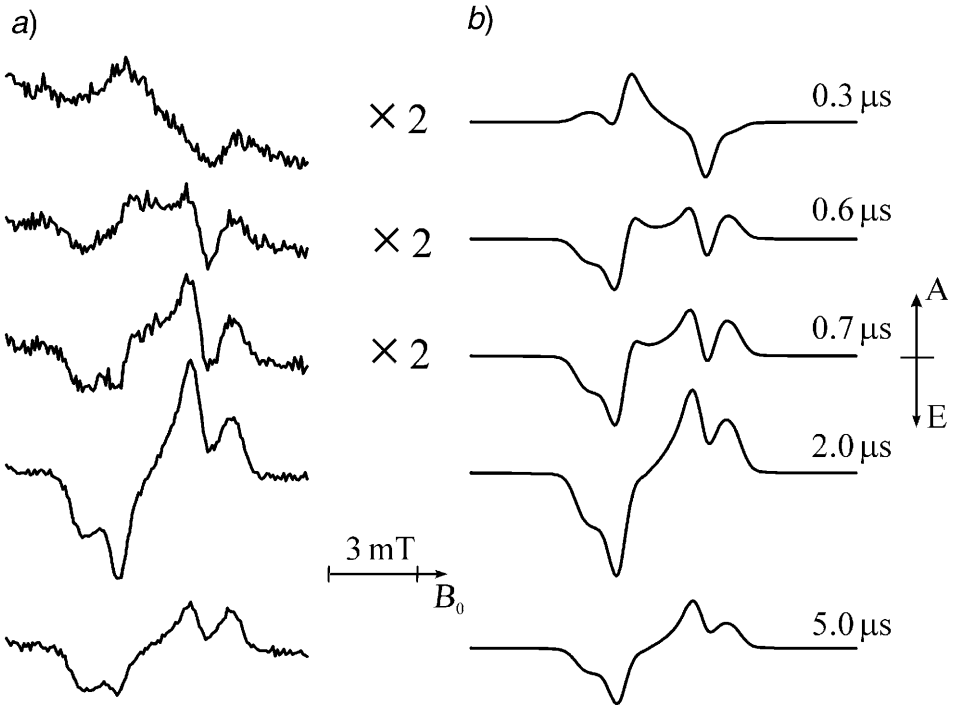


Fig. 10. a) *Time evolution of the X-band TREPR signal of P-*trans*CH-TMQ of* Fig. 9,c (delay times for the measurement after the laser flash are listed on the right side; the integration time was 100 ns). b) *Simulation with the model described in* [39].

*Singlet-Triplet (ST) Mixing*: The state $|T_0\rangle$ in *Fig. 11* is not an eigenstate but is depopulated according to the contribution of $|S\rangle$ to the proper eigenstates and according to the singlet recombination rate $k_{SRC}$. This mechanism cannot depopulate $|T_-\rangle$ and $|T_+\rangle$ simultaneously and, moreover, is strongly field-dependent. Therefore, it cannot cause the observed spin polarization.

*Spin–Orbit Coupling*: According to the nonvanishing electronic matrix element of the spin–orbit operator between the RP triplet and the RP singlet ground state, it is possible that electron charge recombination takes place also directly from the RP triplet states [103]. This mechanism may act selectively on the three triplet states and, thus, might cause spin polarization. It is strongly dependent on the D–A distance and on the environment. It is not only needed that there is a large overlap of the wave functions involved, but there must be also a heavy nucleus nearby in order to produce noticeable spin–orbit coupling. Since this is not the case for our systems, this mechanism probably does not operate efficiently in the nearly planar PQ systems with interradical distances as large as 1–1.5 nm.

*Spin Relaxation*: In a stable spin system, stochastic mixing of states drives the system to thermal equilibrium by spin–lattice relaxation. In a transient spin system, such as a light-generated RP whose lifetime is restricted by rapid charge recombination, the same mechanisms might produce spin polarization [104]. Stochastic modulation of

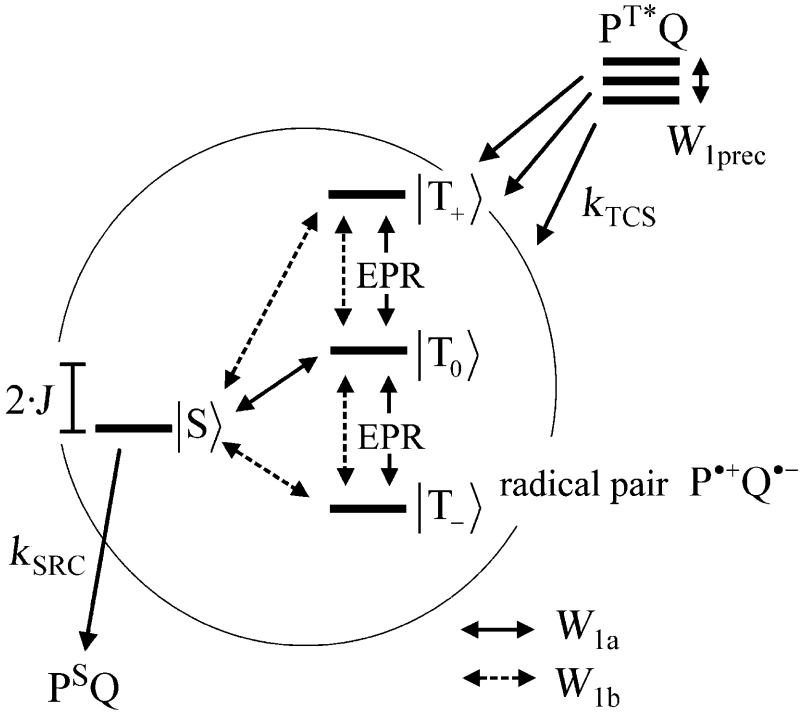


Fig. 11. *States and population/depopulation pathways for a strongly coupled radical pair.* Only the pathways for uncorrelated spin–lattice relaxation $W_{1a}$ and $W_{1b}$ are shown. $k_{SRC}$ = singlet recombination rate; $k_{TCS}$ = triplet charge-separation rate; $J$ = exchange coupling; $W_{1prec}$ = precursor spin–lattice-relaxation rate; $P^SQ$ = PQ ground state; $P^{T*}Q$ = excited triplet state of P. For details, see [39].

the dipolar coupling leads to correlated relaxation, *i.e.*, it connects the triplet states. Modulation of the exchange interaction $J$ leads to transitions between $|S\rangle$ and $|T_0\rangle$. On the other hand, modulation of local interactions that are different for the two electron spins, leads to uncorrelated relaxation, *i.e.*, to singlet–triplet transitions indicated as $W_{1a}$ and $W_{1b}$ in *Fig. 11* [104]. Basically, these two rates are different and, because of the rapid electron recombination from $|S\rangle$, spin polarization in the RP is generated. Both the transition energies and the spin–lattice relaxation may depend on the orientation of the molecule with respect to the magnetic field. This is either because the magnetic interaction of the relaxation mechanism is orientation-dependent or because parts of the molecule undergo anisotropic small-angle fluctuations. This would result in the characteristic orientation-dependent spin polarization which is shown in *Fig. 11*. Hence, we conclude that the observed spin polarization is mainly due to anisotropic spin–lattice relaxation. Indeed, the simulations calculated by using orientation-dependent relaxation rates give very satisfying agreement. For the parameters used in the simulations, see [39].

The value of the exchange interaction $J$ is crucial for the interpretation of the spectra. The semi-empirical predictions for the distance dependence of $J(r)$ are not very helpful in our case: In the through-space model, an exponential dependence

$J(r) = J_0 \cdot \exp[-\delta \cdot (r - r_1 - r_2)]$ is assumed ($r_i$ are the radii of the molecules). P and Q in our systems have distances of 0.98 nm to 1.5 nm. Thus, from the distance dependences published, $|J|$ might be between 0 and $10^4$ mT (!) (see ref. in [101]). On the other hand, it was shown that in the case of a weakly interacting radical pair, one expects an EPR lineshape with different spectral contributions from the pair partners and, moreover, a significant change between X- and W-band spectra. This is not observed, while for a strongly interacting radical pair, one can easily understand the experimental results described. To reach the limit of strong interaction, singlet and triplet states of the radical pair must be separated by at least 50 mT. In *Fig. 10*, the simulated time development of the EPR signals is compared to that of the experiment. The simulations in *Fig. 10*, *b* reproduce the transition from the early AE spectrum to the EEAA spectrum at later times.

We conclude that, with the model and parameters presented in [39], lineshape and time development of the TREPR spectra can be well simulated. The value of the exchange interaction is not critical as long as $|S\rangle$ is energetically separated from $|T_0\rangle$ and $|T_-\rangle$ by at least 50 mT, and as long as the radical pair is strongly coupled. The orientation selection of the PQ systems in the liquid crystal *E7* (*Merck*, UK) was used to directly measure the anisotropy of the spin polarization. The TREPR spectra obtained in a liquid crystal give further evidence for the spin polarization scheme presented. For details, see [39].

4.2.2.3. *Orientation-Dependent Spin-Rotation Relaxation.* In the previous section, it was discussed why in the radical pair of the 'bulky' PQs spin relaxation is most probably responsible for the observed electron-spin polarization. TREPR spectra of RPs could be obtained both in the entire nematic phase of the liquid crystal *E7* as well as in organic solvents in a small temperature range below their melting points. *Earle et al.* [105] have shown that in this situation, molecular motion can be described as a slow diffusion of the solvent cage and a fast diffusion of the molecules in the potential of the solvent cage. Furthermore, they have shown that the *Einstein–Stokes–Debye* relation between temperature, viscosity, and reorientational correlation time is valid down to temperatures that are *ca.* 20% higher than the glass-transition temperature. In highly viscous solvents, the main contribution to spin–lattice relaxation is caused by stochastic modulation of the spin–rotation interaction [106][107]. The spin–rotation interaction Hamiltonian for the spin $\hat{\mathbf{S}}_2$ localized on the quinone site is given by *Eqn. 15*, with the angular momentum $\mathbf{J}$. The tensor $\mathbf{C}$ is related to the $g$ tensor by $\mathbf{C} = -2 \cdot \mathbf{A} \cdot (\mathbf{g} - g_e \cdot \mathbf{1}) \cdot \hbar^2$, where $\mathbf{A}$ denotes the rotational tensor. The spin $\hat{\mathbf{S}}_1$ localized on the porphyrin site is not subject of spin-rotational interaction, because the $g$ tensor of $P^{\bullet+}$ is very close to that of the free electron. Generally, the correlation time $\tau_J$ of the angular momentum is much smaller than the reorientation correlation time $\tau_R$ and we can neglect the modulation of $\mathbf{C}$. In [39], it is shown that the observed spin relaxation is caused by spin–rotation relaxation and anisotropic motion of the molecular fragments.

$$\hat{H}_{SR} = \mathbf{J} \cdot \mathbf{C} \cdot \hat{\mathbf{S}}_2 \tag{15}$$

4.2.2.4. *Model for 'Nonbulky' PQs.* It was rather surprising when it was observed that both W-band and X-band TREPR spectra of P-*trans*CH-BQ in frozen polar solvents are totally emissive (*Figs. 9*, *a* and *b*), *i.e.*, for most molecular orientations, both

transitions in *Eqn. 6* are emissive. Generally, this may be caused by ST_ mixing and fast singlet electron recombination. ST_ Mixing is most effective when $|S\rangle$ and $|T_-\rangle$ are degenerate or at least energetically close. Therefore, because the spectra are emissive in both frequency bands and corresponding magnetic fields, the exchange interaction must be modulated over a wide range. Whether this mechanism leads to emissive spectra or to EEAA spectra depends on the amplitude of the motion. It is restricted by forces within the molecule and between the quinone and the solvent cage. The potential well set up by these forces is increased upon cooling or by substitution with the Me group in the 'bulky' PQ (*e.g.*, P-*trans*CH-TMQ, see *Fig. 7*). In this situation, ST_ mixing is no longer active. In [39], a description of this diffusion model is presented that leads to a consistent interpretation of the TREPR spectra of nonbulky PQs both at X- and W-band. The modulation of *J* must take place on an intermediate time scale within two limits: It must be fast enough that every PQ molecule could adopt a conformation for which $|S\rangle$ and $|T_-\rangle$ are energetically close in both frequency bands before the TREPR signal is observed. On the other hand, the rotational diffusion must be slow enough that the ST_ mixing has time enough to evolve.

4.2.2.5. *Molecular Dynamics of PQ Systems.* From the TREPR study described, the following qualitative conclusions can be drawn: The observed spin polarization is caused by two different mechanisms for bulky and nonbulky PQs. They are related to the two different molecular motions shown in *Fig. 12*.

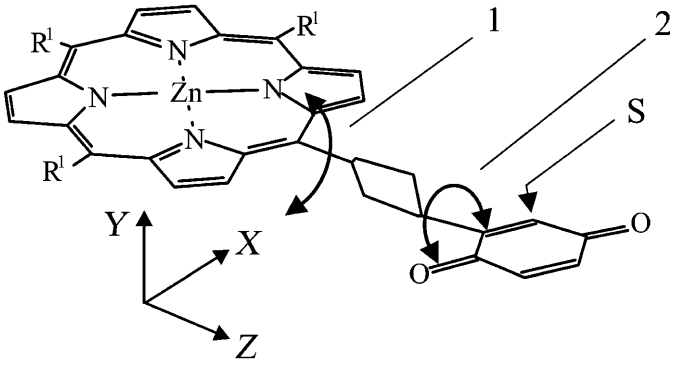


Fig. 12. *Stochastic motions of PQ dyads: Motion of* Type 1 *is active in bulky PQs, and motion of* Type 2 *is active in nonbulky PQs.* Substitution of position S with a Me group renders the system bulky.

Type-1 *Motion*: The PQs have enough flexibility to allow, in the solvent cage, for small-angle fluctuations about an axis parallel to the molecular *X*-axis. The excursion is very small, *i.e.*, the potential well is rather deep. An estimate of the correlation time yields values between $3 \cdot 10^{-11}$ and $2 \cdot 10^{-10}$ s. This is similar to results from measurements on triplet states of porphyrins with their planar structure being distorted by substituents. The X-ray structures of different PQs gives additional evidence for the suggested motional effect: The structures of PQs that only differ at the quinone sites, show slightly different twist angles of the bond between porphyrin and the cyclohexane-1,4-diyl spacer (*e.g.*, P-*trans*CH-BQ, P-*cis*CH-BQ [108], P-*trans*CH-MQ [109]).

Therefore, this bond is probably flexible enough to allow for the molecular motion in question. The temperature dependence of the suggested effect is much less pronounced than one would expect from the *Einstein–Stokes–Debye* relation. The effect is visible over the whole temperature range in which the RP state is observed, and as long as motion of *Type 2* (see below) is not active. This is the case for the bulky PQs which have a Me substituent at point S in *Fig. 12*. This also holds for the nonbulky systems, both dyads and triads, in polar solvent at the lower limit of the temperature range and in liquid crystals.

Type 2 *Motion*: The rotation of the quinone plane with respect to the porphyrin plane is the only motion that can modulate *J* over the necessary range of values and that would be affected by the substitution at point S (*Fig. 12*). Therefore, it is most probable that rotational diffusion about the bond axis between quinone and cyclohexane-1,4-diyl takes place with correlation times $\tau < 10^{-6}$ s for nonbulky PQs at the upper limit of the temperature range for which the RP state is observed. This motion has a strong temperature dependence. On cooling down by 10–20°, the potential barrier for the rotation increases by at least a factor of ten. The same effect has substitution at position S of the quinone or the use of a liquid crystal as solvent environment. Hence, for this situation, the behavior of all PQ systems can be understood in terms of the motion of *Type 1*.

In the systems discussed here, the porphyrin is linked to the quinone by a cyclohexane-1,4-diyl spacer. PQ Systems which are linked by a phenylene spacer behave differently [100]. In this case, TREPR measurements were only possible in liquid crystals, and the observed lineshapes were inversely polarized. Therefore, it was suggested that the RP polarizations are formed through singlet electron transfer and anisotropic relaxation pathways. In the cyclohexane-1,4-diyl-linked systems, this polarization mechanism depopulates the triplet states, whereas in the phenylene-linked systems, it populates the triplet states. This is a plausible mechanism, but it requires that singlet recombination takes place on the microsecond rather than on the nanosecond time scale.

On the other hand, it is also plausible to assume that molecular flexibility is different for the different spacer. Hence, the TREPR results on the phenylene-linked systems may be explained also by triplet electron transfers, and assuming rotational diffusion about the molecular *Z* axis, *i.e.*, as is the case for motion of *Type 2*. The correlation times, however, must be in a range that permits spin–rotational relaxation to occur, as is the case in the bulky cyclohexane-1,4-diyl-linked systems. Obviously, by means of TREPR measurements alone, the different mechanisms cannot be distinguished, and an ambiguity in the analysis remains.

The lifetime of the charge-separated RP state of *ca.* 5 μs is rather long for systems in which the electrons are separated by only 1–1.5 nm. When comparing this with reaction centers of natural photosynthesis, one should keep in mind that the mechanism which leads to this long lifetime in model PQs is very different from that operating in RCs. Also in photosynthesis, the primary charge-separated radical pair, formed in the first ET step after light irradiation, is electronically strongly coupled, but it is born in the singlet state. A long lifetime of a charge-separated state is achieved by the second ET step to the quinone acceptor $Q_A$ by which the distance between the two unpaired electrons is strongly increased. The $P^{\bullet+}Q_A^{\bullet-}$ radical pair, therefore, is elec-

tronically weakly coupled. In contrast to that, the charge-separated states of the porphyrin–quinone dyad and triad model systems are trapped as triplet states of a strongly coupled RP from which charge recombination to the ground state is spin-forbidden.

Nevertheless, we believe that the covalently linked triad systems represent a good starting point for creating long-lived RP states in model tetrad systems of covalently linked porphyrins and quinones [74]. In such 4-component model systems, an additional ET step is possible resulting in an even larger separation of the two electrons. The longer the lifetimes of the dyad and triad RPs, the higher the probability for the additional electron transfer step. Since the lifetime in the dyad and triad systems is limited by the motion-induced triplet–singlet transitions described above, the important strategy for long lifetimes is to restrict molecular flexibility. On the other hand, a certain degree of molecular flexibility is necessary for the first electron transfer step to take place at all. The challenge for constructing suitable tetrad systems is to allow for enough flexibility to initiate electron transfer, but simultaneously to provide enough rigidity to restrict the lifetime limiting triplet–singlet transitions.

It is interesting to note that in contrast to the covalently bridged systems, a *Watson–Crick* base-paired donor–acceptor system is electronically weakly coupled, but nevertheless shows rather fast electron-separation rates and, with only one electron-transfer step, provides a long-lived RP state [91], see below.

4.2.3 *Photoinduced Electron-Transfer in a Base-Paired Porphyrin–Dinitrobenzene Complex*. Since the discovery of photoinduced electron transfer between bacteriochlorophyll and cytochrome [110], many of the more hotly debated issues in the realm of biological ET have involved questions of how long-range ET proceeds through various noncovalently linked protein pathways [111–114]. To answer such questions, among several different spectroscopies, also TREPR has been applied to study biomimetic model systems wherein the donor and acceptor molecules are tethered together noncovalently *via* H-bonds [90][91][115]. These studies, in conjunction with work on covalently linked models [70][89][102][116] have broadened our knowledge of structure–dynamics–function relationships associated with ET processes. Still, many facets of ET processes remain poorly understood, in particular the role of noncovalent interactions. Work on proteins served to establish that specific H-bonding interactions are critical in achieving long-range D–A electronic coupling [117–119]. Furthermore, studies on model systems revealed that the electronic coupling for ET through H-bonds may be larger than that for comparable processes, mediated by either $\sigma$- or $\pi$-bonding networks [120]. Here, we review a first study that combines time-resolved X-band (9.5 GHz, 0.34 T) and W-band (95 GHz, 3.4 T) EPR of a photoexcited *Watson–Crick* base-paired D–A complex [91]. It demonstrates how the critical supramolecular geometry and the ET pathways are stabilized by multiple H-bonding interactions. TREPR Experiments at high *Zeeman* fields, with significantly improved spectral and time resolution, allow us to directly identify the partners of the charge-separated radical pair generated by selective light excitation and to determine unambiguously the genesis of the spin-correlated coupled radical pair in the ET reaction. In the reviewed study, the focus is on X- and W-band TREPR experiments on the base-paired system shown in *Fig. 13*. It consists of a guanine-functionalized porphyrinatozinc ([ZnP]) linked to a cytosine-functionalized dinitrobenzene (DN) *via* noncovalent base-pairing interactions {[ZnP]$\cdots$DN} [90]. A mixture of [ZnP] and DN was dissolved ($5\cdot10^{-4}$ M) in the liquid crystal *E7* (*Merck*,

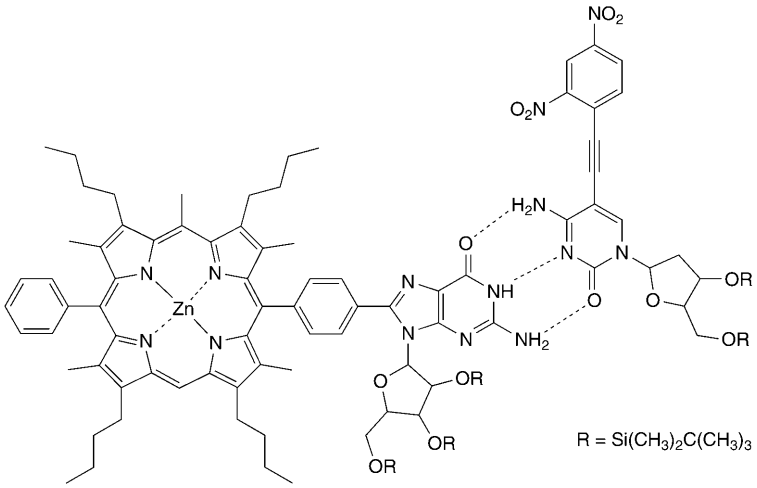


Fig. 13. Watson–Crick-*type base-paired porphyrin-dinitrobenzene complex*

UK) and the solution transferred into a thin-walled quartz capillary and flushed with Ar. Selective pulsed laser excitation (532 nm, 2 mJ, 5 ns) of the porphyrin part in {[ZnP]···DN} results in long-range triplet-initiated ET to the dinitrobenzene, *ca.* 18 Å apart, in the nematic phase of the LC [90][115]. The transient paramagnetic species in *Eq. 16* are TREPR detected in their absorption (A) or emission (E) modes shortly (nanoseconds to microseconds) after the laser pulse to detect them in their spin-polarized states. *Fig. 14,a* shows the X-band TREPR broad and narrow spin-polarized signals, which are ascribed to $^{3}$*[ZnP] and to the RP $^{3}${[ZnP]$^{\bullet+}$···DN$^{\bullet-}$}, respectively [90]. The narrow derivative-like AE signal (*Fig. 14,b*) is assigned to a weakly coupled but still spin-correlated RP, originating from photoinduced triplet-initiated ET, (*Eq. 16*). This assignment is based on CCRP theory of a weakly coupled RP [40][121], see above. For small values of zero-field splitting $D$ and of exchange parameters $J$, as compared to the RP's EPR linewidth, a derivative-like signal is predicted for X-band EPR whose phase pattern, absorption or emission, should depend on the molecular orientation of the RP with respect to the magnetic field. Indeed, when changing the direction of the LC axis and, thereby, the RP molecular orientation by $\pi/2$, it is observed that the phase pattern changes from AE to EA, which is typical for the CCRP case. Such findings are in contrast to the strongly coupled triplet RP case with relatively large $|D|$ and $|J|$ values [39][40].

$$\{[\mathrm{ZnP}]\cdots\mathrm{DN}\} \xrightarrow{h\nu} \{^{*}[\mathrm{ZnP}]\cdots\mathrm{DN}\} \xrightarrow{\mathrm{ISC}} \{^{3*}[\mathrm{ZnP}]\cdots\mathrm{DN}\} \xrightarrow{\mathrm{ET}} {}^{3}\{^{*}[\mathrm{ZnP}]^{\bullet+}\cdots\mathrm{DN}^{\bullet-}\} \quad (16)$$

The X-band EPR method for differentiating between weak and strong exchange coupling is, admittedly, rather ambiguous and asks for an independent, more direct high-field TREPR confirmation. Also, the question remained open whether the derivative-like line consists of contributions from both radicals of the pair or from only one. To identify the partners of the RP and their interactions and clarify the origin of the narrow spin-polarized signal, W-band high-field EPR experiments (10-ns time resolu-

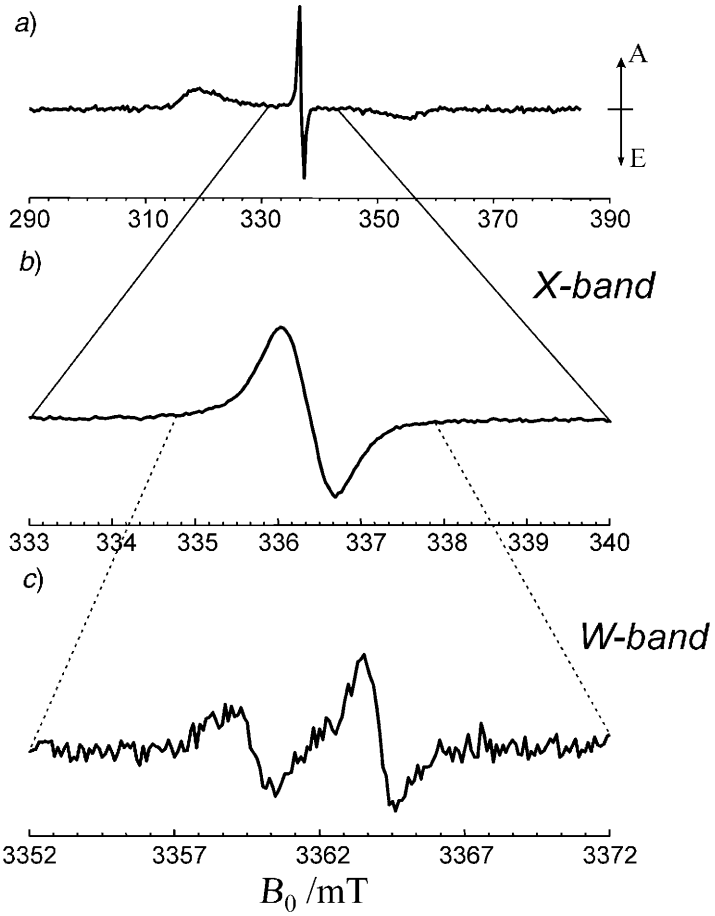


Fig. 14. a) *X-Band AE TREPR spectra of {$^3$[ZnP]···DN} and the superimposed RP $^3${[ZnP]$^{\bullet+}$···DN$^{\bullet-}$}* (narrow signal), *taken in the nematic phase of the liquid crystal* E7 *at 298 K, 450 ns after the laser pulse* [90]. b) *Expanded X-band TREPR spectrum of the RP* [90]. c) *W-Band TREPR spectrum of the RP, taken 250 ns after the laser pulse at 280 K in E7* [91].

tion) were carried out [91]. *Fig. 14,c* shows the spin-polarized RP W-band spectrum with two resolved AE features. In fact, for a weakly coupled RP in disordered samples, CCRP theory [40][121] predicts, as for the general case, a pair of derivative-like lines. The line separation is field-dependent and, at a given $B_0$ field, is determined by the difference in $g$ factors of the two radicals in the CCRP, while the splitting of the antiphase components of the individual derivative-like lines is defined by the dipolar and exchange interactions. The isotropic $g$ factors of $[ZnP]^{\bullet+}$ and $DN^{\bullet-}$ are $2.0025 \pm 0.0003$ [122] and $2.0049 \pm 0.0003$ [123], respectively. At X-band, their $\Delta g$ corresponds to a line separation of 0.42 mT that remains unresolved because of the larger dipolar coupling ($|D| = 0.47$ mT for $\{[ZnP]^{\bullet+}\cdots DN^{\bullet-}\}$) and larger inhomogeneous linewidths [90]. At W-band, however, for a weakly coupled CCRP such as the present one, it is expected that two well-resolved AE lines, separated by 4.2 mT, would be

observed. For a strongly coupled triplet pair, on the other hand, only one line would be expected, even at high field. As can be seen from *Fig. 14*, *c*, a weakly coupled RP spectrum with two separated AE features of both radicals is indeed observed for the base-paired ensemble studied. This confirms that light-induced ET proceeds in the steps postulated by *Eqn. 16*. *Fig. 15* depicts the time evolution of the W-band TREPR spectra. At early times after the laser pulse, two derivative-like AE lines are observed centered around $2.0052 \pm 0.0001$ and $2.0025 \pm 0.0001$. This is in close agreement with the literature values cited above and exactly what CCRP theory predicts for a weakly coupled $\{[ZnP]^{\bullet+} \cdots DN^{\bullet-}\}$ radical pair: The low-field AE line corresponds to the spin-polarized spectrum of $DN^{\bullet-}$, and the high-field AE line to the spin-polarized spectrum of $[ZnP]^{\bullet+}$. The different signal amplitudes are due to different linewidths of the two radicals. The larger linewidth of $DN^{\bullet-}$ is caused by its larger *g* anisotropy, reflecting the orientational distribution of this guest molecule in the liquid crystal. At sufficiently long

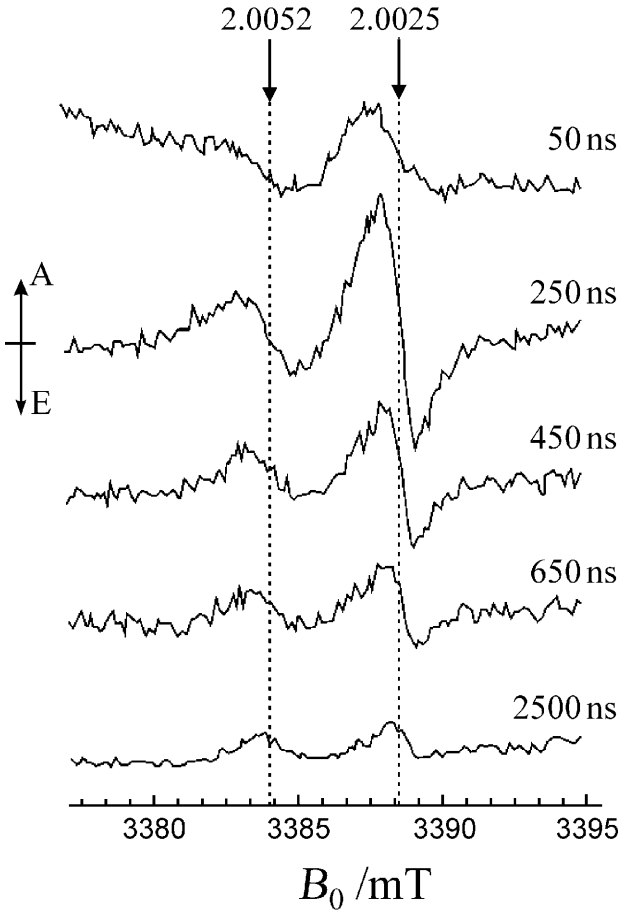


Fig. 15. *W-Band EPR time evolution of the spin-polarized radical-pair spectra at different delay times after the laser pulse* (280 K, in *E7*). The different *g* factors are indicated [91].

times after the laser pulse, the AE lines turn into features characteristic of an absorption spectrum (*Fig. 15*). This time evolution is ascribed to the CCRP undergoing relaxation to a state of thermal equilibrium, with a spin–lattice relaxation time $T_1$ of *ca.* 100 ns. This relaxation, therefore, competes with the building-up of the TREPR spectrum with an ET time constant of *ca.* 50 ns. This means that back ET must be slower than several microseconds. To summarize: The reviewed study [91] has demonstrated that high-field time-resolved EPR opens a new direction in straightforward elucidation of complex photochemical ET reactions, where different paramagnetic states and species are involved. This conclusion applies not only to base-paired donor–acceptor supramolecular ensembles as described here but also to the large ET proteins, such as photosynthetic reaction centers [96][124] and their covalently linked D–A model systems [102].

4.3. *95-GHz EPR on the Spin-Correlated Radical Pair $P^{\bullet+}_{865}Q^{\bullet-}_{A}$ in Bacterial Photosynthesis.* Photosynthesis is the process that enables life on Earth by converting the energy of sunlight into electrochemical energy needed by higher organisms for synthesis, growth, and replication. The so-called primary processes of photosynthesis are those in which the incoming light quanta have initiated electron-transfer reactions between protein-bound donor and acceptor pigments across the cytoplasmic membrane. The successive charge-separating ET steps between the various redox partners in the transmembrane reaction center protein complex have very different reaction rates, $k_{ET}$. The lifetimes, $t_{1/2}=(k_{ET})^{-1}$, of the transient charge-separated states range from less than 1 ps for neighboring D–A pigments to more than 1 ms for large D–A separations on opposite sides of the membrane (*ca.* 40 Å). The cascade of charge-separating ET steps of primary photosynthesis competes extremely favorable with wasteful charge-recombination ET steps, thereby providing almost 100% quantum yield. The largest impact of photosynthesis on life on Earth is due to green plants and certain algae in whose RCs a reversible ET photocycle occurs for which water serves as electron donor. Carbon dioxide is fixed in the form of carbohydrates, and oxygen gas is released as a by-product thereby stabilizing the composition of the Earth's atmosphere.

Three billion years before green plants evolved, photosynthetic energy conversion could be achieved by certain bacteria, for instance the purple bacterium *Rhodobacter* (*Rb.*) *sphaeroides.* These early photosynthetic organisms are simple, one-cellular protein-bound donor–acceptor complexes that contain only one RC for light-induced charge separation. They cannot split $H_2O$, but can reduce $CO_2$ to carbohydrates with the help of sunlight and bacteriochlorophylls and quinones as biocatalysts.

In *Fig. 16*, the structural arrangement of the RC of *Rb. sphaeroides* is shown according to high-resolution X-ray structures [125–128]. The cofactors are embedded in the L, M, H protein domains forming two ET branches, A and B. The RC of the carotenoidless strain R26 of *Rb. sphaeroides* contains nine cofactors: the primary donor $P_{865}$ 'special pair' (a bacteriochlorophyll *a* (BChl) dimer), two accessory BChls ($B_A$, $B_B$), two bacteriopheophytins *a* (BPhe: $H_A$, $H_B$), two ubiquinones ($Q_A$, $Q_B$), one non-heme iron ($Fe^{2+}$).

As a dominant *motif* in the evolution of photosynthetic bacteria, an approximate $C_2$ symmetry of the cofactor arrangement prevails in the RC. It is intriguing that, despite the apparent two-fold local symmetry of the cofactor arrangement, the primary ET pathway is one-sided along the A branch, as indicated by the arrows in *Fig. 16*. The ori-

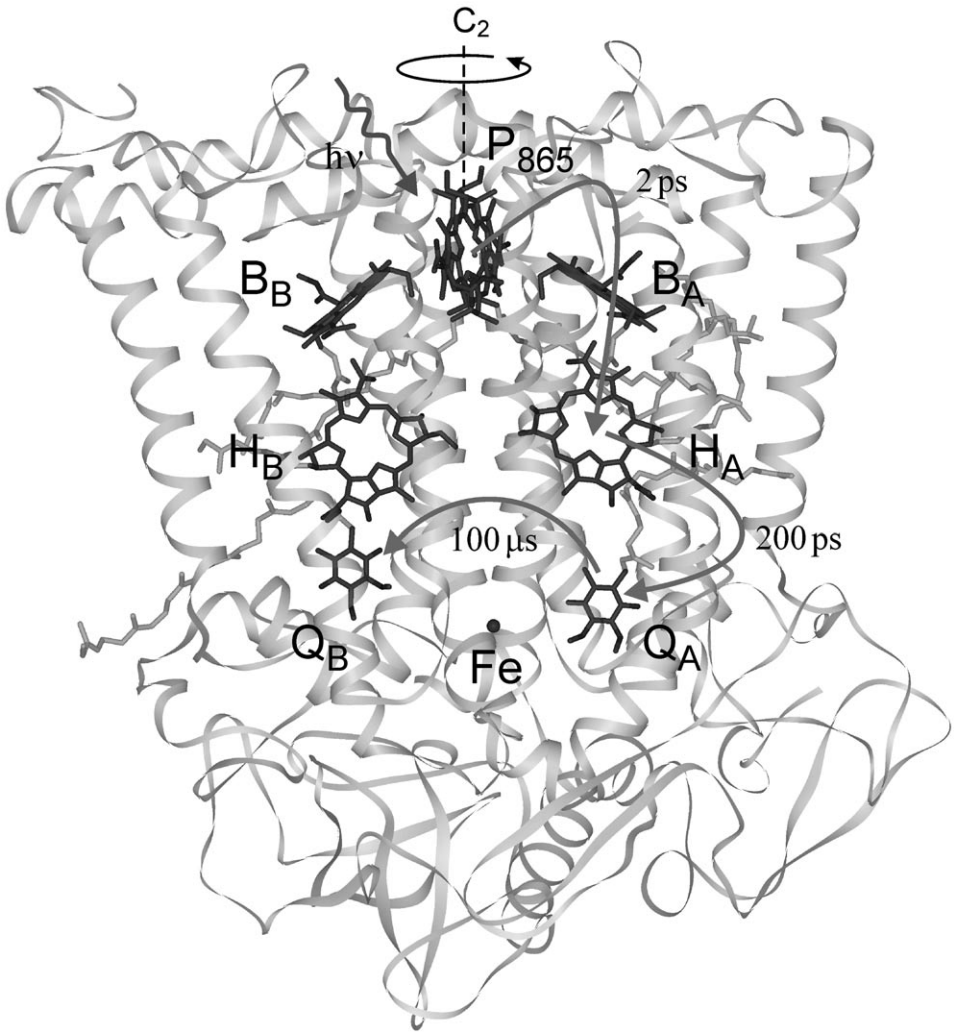


Fig. 16. *X-Ray structural model of RC from* Rb. sphaeriodes [125] *with three protein functional subunits* (L,M,H) *and cofactors* $P_{865}$*, B, H, Q, and Fe.* Light-induced electron transfer proceeds exclusively along the A branch of the cofactors despite the approximate $C_2$ symmetry of the cofactor arrangement. The ET time constants of the charge separation steps are indicated. For details, see text.

gin of this 'unidirectionality' of bacterial ET is not fully understood despite the numerous elaborate studies, both experimentally and theoretically, performed over the last decades. It is, however, clear by now that the ET pathway is largely due to the finely tuned energetics and electronic couplings of the primary donor and the intermediary acceptors (for further reading, see reviews [38][85][129]).

In the following, we review pulsed W-band high-field electron-spin-echo (ESE) experiments on the laser-pulse-generated short-lived $P^{+}_{865}Q^{-}_{A}$ radical pair in frozen RC solution of *Rb. sphaeroides* [96]. These experiments were performed with the

aim to determine, *via* spin-polarization effects, the three-dimensional structure of the charge-separated donor–acceptor system. This excited-state structure might differ from the ground-state structure and, indeed, upon illumination of RC crystals of *Rb. sphaeroides*, drastic changes have been observed in the X-ray structure of the secondary quinone ($Q_B$) binding site in comparison with the dark-adapted X-ray structure [125].

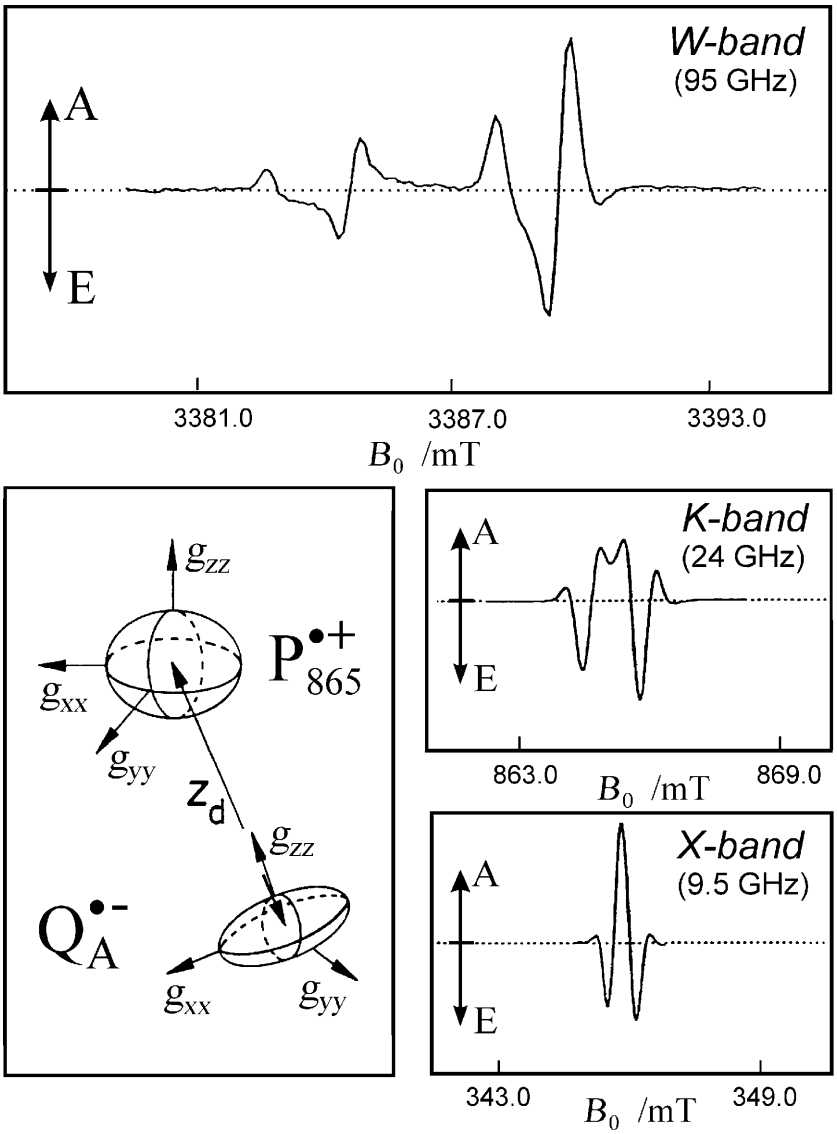


Fig. 17. *Schematic representation of the relative orientation of the* g *tensors and dipolar axis* $z_d$ *of the transient radical pair* $P^+_{865}$ $Q^{\bullet-}_A$ *in deuterated frozen RC solution from* Rb. sphaeroides. The spin-polarized EPR spectra are recorded at various settings of mw frequency and *Zeeman* field. A and E stand for absorption and emission, respectively. For details, see [96].

The high-field EPR spectra were recorded by using the field-swept two-pulse ESE technique. To avoid fast spin relaxation of the $Q_A^{\bullet-}$, the non-heme $Fe^{2+}$ ion was replaced by $Zn^{2+}$. The charge-separated radical pairs $P_{865}^{\bullet+}Q_A^{\bullet-}$ were generated by 10-ns laser flashes. Their time-resolved EPR spectrum is strongly electron-spin polarized because the transient RPs are suddenly born in a spin-correlated non-eigenstate of the spin Hamiltonian with pure singlet character. Such spin-polarized spectra with lines in enhanced absorption and emission (see *Fig. 17*) originate from the CCRP mechanism described in the previous sections. They contain important structural information of magnitude and orientation of the *g* tensors of the two radical partners, $P_{865}^{\bullet+}$ and $Q_A^{\bullet-}$, with respect to each other and to the dipolar axis $z_d$ connecting the two radicals (see *Fig. 17*). Several parameters critically determine the lineshape of the CCRP polarization pattern, such as the principal values and orientations of the *g* and electron dipolar-coupling tensors, the exchange coupling *J*, and the inhomogeneous linewidths of both radicals [96]. From earlier time-resolved EPR measurements on $P_{865}^{\bullet+}Q_A^{\bullet-}$ at X-band (9.5 GHz), K-band (24 GHz), and Q-band (35 GHz), *g* tensor orientations could not be extracted unambiguously from spectra simulations (for ref., see [130]). This was mainly because of strongly overlapping lines, even when deuterated samples were used to reduce hyperfine contributions. In the pulsed W-band ESE experiments, however, the *Zeeman* field is strong enough to largely separate the spectral contributions from $P_{865}^{\bullet+}$ and $Q_A^{\bullet-}$. Thus, the overall spectrum is dominated by the characteristics of the two *g* tensors, and its interpretation is simplified. It allows for an unambiguous analysis of the tensor orientations. The most important result of this high-field ESE study is that, within an error margin of $\pm 0.3$ Å, no light-induced structural changes of the $Q_A^{\bullet-}$ site with respect to $P_{865}^{\bullet+}$ occur, as compared to the ground-state configuration $P_{865}Q_A$. This finding is in accordance with recent results from various other studies, including X-ray crystallography [125], and contrasts with the $Q_B^{\bullet-}$ situation.

We conclude that by time-resolved high-field EPR, such as pulsed ESE experiments, on spin-correlated coupled radical pairs, a detailed picture of the electronic structure and spin dynamics of the ET partners can be obtained. Moreover, ET-induced structural changes in the relative orientation of donor and acceptor can be detected with high precision, even for disordered samples. Such information is important for a deeper understanding of the ET characteristics of charge-separation and charge-recombination processes on the molecular level. The charge-separated RP state represents the initial state for ET recombination, *i.e.*, it is one of the important working states of the photocycle in the photosynthetic RC.

**5. Conclusions.** – In this overview, it is shown that modern multifrequency EPR spectroscopy, in particular at high magnetic fields, provides detailed information about structure, dynamics, and spin chemistry of transient radicals and radical pairs occurring in photochemical reactions in liquid solution as well as in light-induced electron-transfer processes in biomimetic donor–acceptor model systems in frozen solution and liquid crystals and in natural photosynthetic-reaction-center protein complexes. The transient paramagnetic states detected after photoinitiation of the reaction often show characteristic electron-polarization (CIDEP) effects which not only contain valuable information about structure and dynamics of the transient reaction intermediates, but can also be exploited for signal enhancement. The cw or pulsed versions of

time-resolved high-field EPR spectroscopy are compared with respect to their advantages and limitations for the specific system under study, and examples for cw transient EPR (TREPR) and pulsed-electron spin echo (ESE) experiments at FU Berlin are presented.

For instance, W-band (95 GHz) TREPR spectroscopy in conjunction with a continuous-flow system for light-generated short-lived transient radicals of organic photoinitiators in solution was performed. The high time resolution of W-band EPR of 10 ns combined with the high detection sensitivity allows one to record even weak transient signals on a much shorter time scale than conventional X-band EPR can provide (100 ns). The increased *Boltzmann* polarization at high fields even allows detection of transient radicals without CIDEP effects. This enables one to determine initial radical-polarization contributions as well as radical addition reaction constants.

Another example of the power of combined X-band and W-band TREPR spectroscopy is given for the complex electron-transfer and spin dynamics of covalently linked porphyrin–quinone as well as *Watson–Crick* base-paired porphyrin–dinitrobenzene donor–acceptor biomimetic model systems. Furthermore, W-band ESE experiments on the spin-correlated coupled radical pair $P^{\bullet+}_{865}Q^{\bullet-}_{A}$ in reaction centers of the purple photosynthetic bacterium *Rb. sphaeroides* reveal details of distance and orientation of the pair partners in their charge-separated transient state in comparison with the ground-state $P_{865}Q_A$. The high orientation selectivity of high-field EPR provides single-crystal like information even from disordered frozen-solution samples.

Below, some summarizing conclusions are given with emphasis on biological samples: 1. Many organic cofactors in proteins have only small *g* anisotropies and, therefore, require much higher magnetic fields than available in X-band EPR to resolve the canonical *g* tensor orientations in their powder spectra. Thereby, even on disordered samples, orientation-selective H-bonding and polar interactions in the protein binding sites can be traced.

2. In electron-transfer processes, often several organic radical species are generated as transient intermediates. To distinguish them by the small differences in their *g* factor and hyperfine interactions, high *Zeeman* fields are required and, hence, high-frequency EPR becomes the method of choice.

3. Often high-purity protein samples can be prepared only in minute quantities, for example site-directed mutants or isotopically labelled cofactors. Accordingly, to study them by EPR, very high detection sensitivity is needed, which often can be accomplished only by dedicated high-field/high-frequency spectrometers.

4. High-field/high-frequency cw EPR generally provides, by lineshape analysis, shorter time windows down into the picosecond range for studying correlation times and fluctuating local fields over a wide temperature range. They are associated with characteristic dynamic processes, such as protein and cofactor motion.

5. Pulsed high-field/high-frequency EPR as, for example, two-dimensional field-swept ESE spectroscopy, provides real-time access to specific cofactor and/or protein motions on the nanosecond time scale. Motional anisotropy can be resolved which is governed by anisotropic interactions, such as H-bonding along specific molecular axes within the binding site.

6. High-field EPR adds substantially to the capability of 'classical' spectroscopic and diffraction techniques for determining structure–dynamics–function relations of

biosystems, since transient intermediates can be observed in real time in their *working states* on biologically relevant time scales.

Over the years, numerous co-workers and cooperation partners from many parts of the world have contributed to the high-field EPR work presented in this special issue in memory of *Hanns Fischer*. To all of them, we want to express our gratitude. Their individual share in the work becomes evident by the references cited. Financial support by the *Deutsche Forschungsgemeinschaft* (DFG priority program SPP 1051, DFG collaborative research center SFB 498, MO 132/19–2) is gratefully acknowledged.

## REFERENCES

[1] W. T. Dixon, R. O. C. Norman, *Nature (London)* **1962**, *196*, 891.
[2] H. Fischer, *Z. Naturforsch., A* **1964**, *19*, 866.
[3] R. Livingston, H. Zeldes, *J. Chem. Phys.* **1966**, *44*, 1245.
[4] H. Paul, H. Fischer, *Helv. Chim. Acta* **1973**, *56*, 1575.
[5] H. Paul, H. Fischer, *Z. Naturforsch., A* **1970**, *25*, 443.
[6] B. Smaller, J. R. Remko, E. C. Avery, *J. Chem. Phys.* **1968**, *48*, 5174.
[7] R. Kaptein, J. L. Oosterhoff, *Chem. Phys. Lett.* **1969**, *4*, 195.
[8] R. Kaptein, J. L. Oosterhoff, *Chem. Phys. Lett.* **1969**, *4*, 214.
[9] G. L. Closs, *J. Am. Chem. Soc.* **1969**, *91*, 4552.
[10] H. Fischer, *Chem. Phys. Lett.* **1970**, *4*, 611.
[11] T. N. Makarov, A. N. Savitsky, K. Möbius, D. Beckert, H. Paul, *J. Phys. Chem. A* **2005**, *109*, 2254.
[12] A. N. Savitsky, M. Galander, K. Möbius, *Chem. Phys. Lett.* **2001**, *340*, 458.
[13] P. Jaegermann, F. Lendzian, G. Rist, K. Möbius, *Chem. Phys. Lett.* **1987**, *140*, 615.
[14] F. Lendzian, P. Jaegermann, K. Möbius, *Chem. Phys. Lett.* **1985**, *120*, 195.
[15] K. Möbius, K. Hoffmann, M. Plato, *Z. Naturforsch., A* **1968**, *23*, 1209.
[16] J. H. Van der Waals, M. S. de Groot, in 'The Triplet State', Ed. A. B. Zahlan, Cambridge University Press, Cambridge, 1967, p. 101.
[17] S. Yamauchi, D. W. Pratt, *Mol. Phys.* **1979**, *37*, 541.
[18] S. K. Wong, D. A. Hutchinson, J. K. S. Wan, *J. Chem. Phys.* **1973**, *58*, 985.
[19] F. J. Adrian, *J. Chem. Phys.* **1974**, *61*, 4875.
[20] P. W. Atkins, G. T. Evans, *Chem. Phys. Lett.* **1974**, *25*, 108.
[21] P. W. Atkins, G. T. Evans, *Mol. Phys.* **1974**, *27*, 1633.
[22] J. B. Pedersen, J. H. Freed, *J. Chem. Phys.* **1975**, *62*, 1706.
[23] P. W. Atkins, K. A. McLauchlan, A. R. Lepley, G. L. Closs, in 'Chemically Induced Magnetic Polarization', Wiley, New York, 1973.
[24] F. J. Adrian, *Rev. Chem. Intermed.* **1986**, *7*, 173.
[25] L. Monchick, F. J. Adrian, *J. Chem. Phys.* **1978**, *68*, 4376.
[26] K. M. Salikhov, Y. N. Molin, R. Z. Sagdeev, A. L. Buchachenko, 'Spin Polarization and Magnetic Effects in Radical Reactions', Elsevier, Amsterdam, 1984.
[27] J. H. Freed, J. B. Pedersen, in 'Advances in Magnetic Resonance', Ed. J. S. Waugh, Academic Press, New York, 1976, Vol. 8, p. 1.
[28] F. J. Adrian, *Res. Chem. Intermed.* **1991**, *16*, 99.
[29] A. I. Shushin, J. B. Pedersen, L. I. Lolle, *Chem. Phys.* **1993**, *177*, 119.
[30] F. J. Adrian, *J. Chem. Phys.* **1971**, *54*, 3918.
[31] J. B. Pedersen, J. H. Freed, *J. Chem. Phys.* **1973**, *59*, 2869.
[32] J. B. Pedersen, J. H. Freed, *J. Chem. Phys.* **1973**, *58*, 2746.
[33] A. I. Shushin, *Chem. Phys.* **1990**, *144*, 201.
[34] A. I. Shushin, *Chem. Phys.* **1990**, *144*, 223.
[35] F. J. Adrian, *Chem. Phys. Lett.* **1981**, *80*, 106.
[36] T. J. Burkey, J. Lusztyk, K. U. Ingold, J. K. S. Wan, F. J. Adrian, *J. Phys. Chem.* **1985**, *89*, 4286.
[37] A. D. Trifunac, *Chem. Phys. Lett.* **1977**, *49*, 457.
[38] A. J. Hoff, J. Deisenhofer, *Phys. Rep.* **1997**, *287*, 2.

[39] M. Fuhs, G. Elger, A. Osintsev, A. Popov, H. Kurreck, K. Möbius, *Mol. Phys.* **2000**, *98*, 1025.
[40] P. J. Hore, in 'Advanced EPR, Applications in Biology and Biochemistry', Ed. A. J. Hoff, Elsevier, Amsterdam, 1989, p. 405.
[41] A. J. Hoff, in 'The Photosynthetic Reaction Center', Eds. J. Deisenhofer, J. R. Norris, Academic, San Diego, 1993, Vol. 2, p. 331.
[42] R. Furrer, F. Fujara, C. Lange, D. Stehlik, H. M. Vieth, W. Vollmann, *Chem. Phys. Lett.* **1980**, *75*, 332.
[43] H. van Willigen, P. R. Levstein, M. H. Ebersole, *Chem. Rev.* **1993**, *93*, 173.
[44] J. H. Freed, *Ann. Rev. Phys. Chem.* **2000**, *51*, 655.
[45] K. A. McLauchlan, M. T. Yeung, in 'Electron Spin Resonance', Royal Society of Chemistry, Cambridge, 1994, Vol. 14, p. 32.
[46] M. R. Clancy, V. F. Tarasov, M. D. E. Forbes, in 'Electron Paramagnetic Resonance', Royal Society of Chemistry, Cambridge, 1998, Vol. 16, p. 50.
[47] P. W. Atkins, K. A. McLauchlan, A. F. Simpson, *J. Phys. E* **1970**, *3*, 547.
[48] T. H. Wilmshurst, 'Electron Spin Resonance Spectrometers', Adam Hilger, London, 1967.
[49] C. P. Poole, 'Electron Spin Resonance', J. Wiley, New York, 1983.
[50] A. N. Savitsky, H. Paul, *Appl. Magn. Reson.* **1997**, *12*, 449.
[51] A. N. Savitsky, H. Paul, A. I. Shushin, *J. Phys. Chem. A* **2000**, *104*, 9091.
[52] A. Schweiger, G. Jeschke, 'Principles of Pulse Electron Paramagnetic Resonance', Oxford University Press, Oxford, 2001.
[53] D. Goldfarb, in 'Electron Paramagnetic Resonance', Royal Society of Chemistry, Cambridge, 1996, Vol. 15, p. 182.
[54] D. Hristova, I. Gatlik, G. Rist, K. Dietliker, J. P. Wolf, J. L. Birbaum, A. Savitsky, K. Möbius, G. Gescheidt, *Macromolecules* **2005**, *38*, 7714.
[55] A. Borer, R. Kirchmayr, G. Rist, *Helv. Chim. Acta* **1978**, *61*, 305.
[56] M. R. Sandner, C. L. Osborn, *Tetrahedron Lett.* **1974**, 415.
[57] J. P. Fouassier, A. Merlin, *J. Photochem.* **1980**, *12*, 17.
[58] H. Fischer, R. Baer, R. Hany, I. Verhoolen, M. Walbiner, *J. Chem. Soc., Perkin Trans. 2* **1990**, 787.
[59] F. Jent, H. Paul, H. Fischer, *Chem. Phys. Lett.* **1988**, *146*, 315.
[60] M. D. E. Forbes, *J. Phys. Chem.* **1992**, *96*, 7836.
[61] H.-R. Dütsch, Diploma Thesis, University Zürich, 1975.
[62] A. L. Konkin, H. K. Roth, M. Schroedner, G. A. Nazmutdinova, A. V. Aganov, T. Ida, R. R. Garipov, *Chem. Phys.* **2003**, *287*, 377.
[63] U. Kolczak, G. Rist, K. Dietliker, J. Wirz, *J. Am. Chem. Soc.* **1996**, *118*, 6477.
[64] G. W. Sluggett, P. F. McGarry, I. V. Koptyug, N. J. Turro, *J. Am. Chem. Soc.* **1996**, *118*, 7367.
[65] M. Kamachi, K. Kuwata, T. Sumiyoshi, W. Schnabel, *J. Chem. Soc., Perkin Trans. 2* **1988**, 961.
[66] A. I. Shushin, *Chem. Phys. Lett.* **1990**, *170*, 78.
[67] S. Jockusch, N. J. Turro, *J. Am. Chem. Soc.* **1998**, *120*, 11773.
[68] I. Gatlik, P. Rzadek, G. Gescheidt, G. Rist, B. Hellrung, J. Wirz, K. Dietliker, G. Hug, M. Kunz, J. P. Wolf, *J. Am. Chem. Soc.* **1999**, *121*, 8332.
[69] S. Jockusch, I. V. Koptyug, P. F. McGarry, G. W. Sluggett, N. J. Turro, D. M. Watkins, *J. Am. Chem. Soc.* **1997**, *119*, 11495.
[70] H. Levanon, K. Möbius, *Annu. Rev. Biophys. Biomol. Struct.* **1997**, 26, 495.
[71] J. Kurreck, D. Niethammer, H. Kurreck, *Chem. unserer Zeit* **1999**, *33*, 72.
[72] D. Gust, T. A. Moore, A. L. Moore, *Acc. Chem. Res.* **2001**, *34*, 40.
[73] D. M. Guldi, *Pure Appl. Chem.* **2003**, *75*, 1069.
[74] A. Wiehe, M. O. Senge, A. Schafer, M. Speck, S. Tannert, H. Kurreck, B. Roder, *Tetrahedron* **2001**, *57*, 10089.
[75] E. A. Weiss, M. A. Ratner, M. R. Wasielewski, *J. Phys. Chem. A* **2003**, *107*, 3639.
[76] M. Volk, T. Häberle, R. Feick, A. Ogrodnik, M. E. Michel-Beyerle, *J. Phys. Chem.* **1993**, *97*, 9831.
[77] M. Di Valentin, A. Bisol, G. Agostini, M. Fuhs, P. A. Liddell, A. L. Moore, T. A. Moore, D. Gust, D. Carbonera, *J. Am. Chem. Soc.* **2004**, *126*, 17074.
[78] T. Yago, Y. Kobori, K. Akiyama, S. Tero-Kubota, *J. Phys. Chem. B* **2002**, *106*, 10074.

[79] R. Calvo, E. C. Abresch, R. Bittl, G. Feher, W. Hofbauer, R. A. Isaacson, W. Lubitz, M. Y. Okamura, M. L. Paddock, *J. Am. Chem. Soc.* **2000**, *122*, 7327.
[80] M. Di Valentin, A. Bisol, G. Agostini, D. Carbonera, *J. Chem. Inf. Model.* **2005**, *45*, 1580.
[81] Y. Kandrashkin, M. S. Asano, A. van der Est, *J. Phys. Chem. A* **2006**, in press.
[82] P. W. Anderson, *Phys. Rev.* **1959**, *115*, 2.
[83] R. A. Marcus, *J. Chem. Phys.* **1956**, *24*, 966.
[84] H. Fröhlich, 'Theory of Dielectrics', Oxford University Press, Oxford, 1990.
[85] M. Bixon, J. Fajer, G. Feher, J. H. Freed, D. Gamliel, A. J. Hoff, H. Levanon, K. Möbius, R. Nechushtai, J. R. Norris, A. Scherz, J. L. Sessler, D. Stehlik, *Isr. J. Chem.* **1992**, *32*, 369.
[86] F. Lendzian, B. von Maltzan, *Chem. Phys. Lett.* **1991**, *180*, 191.
[87] K. Hasharoni, H. Levanon, *J. Phys. Chem.* **1995**, *99*, 4875.
[88] A. J. Martin, G. Meier, A. Saupe, *Symp. Faraday Soc.* **1971**, *5*, 119.
[89] H. Levanon, K. Hasharoni, *Prog. React. Kinet.* **1995**, *20*, 309.
[90] M. Asano-Someda, H. Levanon, J. L. Sessler, R. Z. Wang, *Mol. Phys.* **1998**, *95*, 935.
[91] A. Berg, Z. Shuali, M. Asano-Someda, H. Levanon, M. Fuhs, K. Möbius, *J. Am. Chem. Soc.* **1999**, *121*, 7433.
[92] G. P. Wiederrecht, W. A. Svec, M. R. Wasielewski, T. Galili, H. Levanon, *J. Am. Chem. Soc.* **2000**, *122*, 9715.
[93] F. Lendzian, J. Schlüpmann, J. von Gersdorff, K. Möbius, H. Kurreck, *Angew. Chem., Int. Ed.* **1991**, *30*, 1461.
[94] M. C. Thurnauer, J. R. Norris, *Chem. Phys. Lett.* **1980**, *76*, 557.
[95] D. Stehlik, C. H. Bock, J. Petersen, *J. Phys. Chem.* **1989**, *93*, 1612.
[96] T. F. Prisner, A. van der Est, R. Bittl, W. Lubitz, D. Stehlik, K. Möbius, *Chem. Phys.* **1995**, *194*, 361.
[97] G. L. Closs, M. D. E. Forbes, *J. Phys. Chem.* **1991**, *95*, 1924.
[98] N. I. Avdievich, M. D. E. Forbes, *J. Phys. Chem.* **1995**, *99*, 9660.
[99] M. D. E. Forbes, N. I. Avdievich, J. D. Ball, G. R. Schulz, *J. Phys. Chem.* **1996**, *100*, 13887.
[100] G. Elger, H. Kurreck, A. Wiehe, E. Johnen, M. Fuhs, T. Prisner, J. Vrieze, *Acta Chem. Scand.* **1997**, *51*, 593.
[101] K. M. Salikhov, J. Schlüpmann, M. Plato, K. Möbius, *Chem. Phys.* **1997**, *215*, 23.
[102] G. Elger, M. Fuhs, P. Müller, J. von Gersdorff, A. Wiehe, H. Kurreck, K. Möbius, *Mol. Phys.* **1998**, *95*, 1309.
[103] F. J. J. de Kanter, R. Kaptein, *J. Am. Chem. Soc.* **1982**, *104*, 4759.
[104] F. J. J. de Kanter, J. A. den Hollander, A. H. Huizer, R. Kaptein, *Mol. Phys.* **1977**, *34*, 857.
[105] K. A. Earle, J. K. Moscicki, A. Polimeno, J. H. Freed, *J. Chem. Phys.* **1997**, *106*, 9996.
[106] D. S. Leniart, H. D. Connor, J. H. Freed, *J. Chem. Phys.* **1975**, *63*, 165.
[107] J. S. Hwang, R. P. Mason, L. P. Hwang, J. H. Freed, *J. Phys. Chem.* **1975**, *79*, 489.
[108] J. Fajer, K. M. Barkigia, D. Melamed, R. M. Sweet, H. Kurreck, J. von Gersdorff, M. Plato, H. C. Rohland, G. Elger, K. Möbius, *J. Phys. Chem.* **1996**, *100*, 14236.
[109] H. Dieks, Ph.D. Thesis, Free University Berlin, 1996.
[110] B. Chance, M. Nishimura, *Proc. Natl. Acad. Sci. U.S.A.* **1960**, *46*, 19.
[111] S. S. Skourtis, J. N. Onuchic, D. N. Beratan, *Inorg. Chim. Acta* **1996**, *243*, 167.
[112] C. C. Moser, C. C. Page, X. Chen, P. L. Dutton, *J. Biol. Inorg. Chem.* **1997**, *2*, 393.
[113] M. Bixon, J. Jortner, *J. Chem. Phys.* **1997**, *107*, 5154.
[114] J. J. Regan, J. N. Onuchic, in 'The Reaction Centers of Photosynthetic Bacteria', Ed. M. E. Michel-Beyerle, Springer, Berlin, 1996, p. 117.
[115] A. Berman, E. S. Izraeli, H. Levanon, B. Wang, J. L. Sessler, *J. Am. Chem. Soc.* **1995**, *117*, 8252.
[116] J. P. Sumida, P. A. Liddell, S. Lin, A. N. Macpherson, G. R. Seely, A. L. Moore, T. A. Moore, D. Gust, *J. Phys. Chem. A* **1998**, *102*, 5512.
[117] M. J. Therien, M. Selman, H. B. Gray, I. J. Chang, J. R. Winkler, *J. Am. Chem. Soc.* **1990**, *112*, 2420.
[118] R. A. Marcus, *Pure Appl. Chem.* **1997**, *69*, 13.
[119] S. S. Skourtis, D. N. Beratan, in 'Electron Transfer from Isolated Molecules to Biomolecules', Part 1, Eds. J. Jortner and M. Bixon, 1999, p. 377.
[120] P. J. F. Derege, S. A. Williams, M. J. Therien, *Science (Washington, D.C.)* **1995**, *269*, 1409.

[121] G. L. Closs, M. D. E. Forbes, J. R. Norris, *J. Phys. Chem.* **1987**, *91*, 3592.
[122] R. H. Felton, in 'The Porphyrins', Ed. D. Dolphin, Academic Press, New York, 1978, Vol. 5, p. 53.
[123] Landolt-Börnstein, in 'Numerical Data and Functional Relationships in Science and Technology', Ed. K.-H. Hellwege, Springer, Berlin, 1980, Vol. 9, New Series, Group II, Part d1, p. 619.
[124] A. van der Est, T. Prisner, R. Bittl, P. Fromme, W. Lubitz, K. Möbius, D. Stehlik, *J. Phys. Chem. B* **1997**, *101*, 1437.
[125] M. H. B. Stowell, T. M. McPhillips, D. C. Rees, S. M. Soltis, E. Abresch, G. Feher, *Science (Washington, D.C.)* **1997**, *276*, 812.
[126] A. J. Chirino, E. J. Lous, M. Huber, J. P. Allen, C. C. Schenck, M. L. Paddock, G. Feher, D. C. Rees, *Biochemistry* **1994**, *33*, 4584.
[127] J. P. Allen, G. Feher, T. O. Yeates, H. Komiya, D. C. Rees, *Proc. Natl. Acad. Sci. U.S.A.* **1987**, *84*, 5730.
[128] J. P. Allen, G. Feher, T. O. Yeates, H. Komiya, D. C. Rees, *Proc. Natl. Acad. Sci. U.S.A.* **1987**, *84*, 6162.
[129] W. Lubitz, *Phys. Chem. Chem. Phys.* **2002**, *4*, 5539.
[130] D. Stehlik, K. Möbius, *Annu. Rev. Phys. Chem.* **1997**, *48*, 745.
[131] J. Schlüpmann, F. Lendzian, M. Plato, K. Möbius, *J. Chem. Soc., Faraday Trans.* **1993**, *89*, 2853.

*Received August 1, 2006*